Review

International Journal of Modern Physics B
Vol. 18, No. 25 (2004) 3267–3314

World Scientific
www.worldscientific.com

FROM SEAS TO SURGERIES, FROM BABBLING BROOKS TO BABY SCANS: THE ACOUSTICS OF GAS BUBBLES IN LIQUIDS*

T. G. LEIGHTON

Institute of Sound and Vibration Research, University of Southampton, Highfield, Southampton SO17 1BJ, UK
tgl@soton.ac.uk

Received 29 September 2004

Gas bubbles are the most potent naturally-occurring entities that influence the acoustic environment in liquids. Upon entrainment under breaking waves, waterfalls, or rainfall over water, each bubble undergoes small amplitude decaying pulsations with a natural frequency that varies approximately inversely with the bubble radius, giving rise to the "plink" of a dripping tap or the roar of a cataract. When they occur in their millions per cubic metre in the top few metres of the ocean, bubbles can dominate the underwater sound field. Similarly, when driven by an incident sound field, bubbles exhibit a strong pulsation resonance. Acoustic scatter by bubbles can confound sonar in the shallow waters which typify many modern maritime military operations. If they are driven by sound fields of sufficient amplitude, the bubble pulsations can become highly nonlinear. These nonlinearities might be exploited to enhance sonar, or to monitor the bubble population. Such oceanic monitoring is important, for example, because of the significant contribution made by bubbles to the greenhouse gas budget. In industry, bubble monitoring is required for sparging, electrochemical processes, the production of paints, pharamaceuticals and foodstuffs. At yet higher amplitudes of pulsation, gas compression within the collapsing bubble can generate temperatures of several thousand Kelvin whilst, in the liquid, shock waves and shear can produce erosion and bioeffects. Not only can these effects be exploited in industrial cleaning and manufacturing, and research into novel chemical processes, but we need to understand (and if possible control) their occurrence when biomedical ultrasound is passed through the body. This is because the potential of such bubble-related physical and chemical processes to damage tissue will be desireable in some circumstances (e.g. ultrasonic kidney stone therapy), and undesireable in others (e.g. foetal scanning). This paper describes this range of behaviour. Further information on these topics, including sound and video files, can be found at http://www.isvr.soton.ac.uk/fdag/ijmpb.htm.

Keywords: Bubbles; cavitation; acoustics; ultrasound; sonar; cetacean; sonochemistry; erosion; bioeffect; waterfall; lithotripsy; acoustical oceanography; Faraday waves.

*This paper is based on the 2002 Tyndall Medal Address of the Institute of Acoustics.

1. Introduction

The study of bubble acoustics contains a wealth of fascinating physics.[1] The ideal spherical pulsating bubble acts as a damped oscillator: the stiffness comes from the bubble gas (which exerts a restoring force when the bubble volume changes); and the inertia is invested primarily in the surrounding liquid, which is set into motion when the bubble wall moves. Viscous, thermal and acoustic radiation losses contribute to the damping.

As linear oscillators at low amplitudes of pulsation, gas bubbles in liquids are abundant and responsible for many of the sounds that we associate with liquids in the natural world. When driven by external sound fields, a bubble exhibits a powerful pulsation resonance, plus numerous resonances associated with higher-order spherical harmonic shape perturbations. At finite amplitudes, bubbles will not only "process" the driving sound field by generating harmonics, subharmonics and combination frequencies; but they can also process the surrounding medium, producing physical, chemical and biological changes. Furthermore, all these phenomena are not simply interesting in their own right: they can be exploited as tools. As a result, problems in bubble acoustics can sometimes lead to complete solutions, starting with the fundamental physics and ending with a product or device in the clinic, laboratory or market.

2. Acoustic Fields in Liquids

2.1. *Acoustic diagnostics*

Acoustic waves are passed through liquids and tissue both for diagnostic reasons and in order to produce a material change. Whilst there are many examples of the diagnostic uses of ultrasound[2] (e.g. in the nuclear industry[3–8]), this section will discuss the biomedical and oceanographic applications.

In biomedicine, the most familiar diagnostic application is external foetal scanning using 3–30 MHz ultrasound. This is now a routine procedure in many pregnancies in industrialised nations. However, many more anatomical sites are now benefiting from ultrasonic scanning.[9] Innovations include the development of probes for use whilst inserted into body cavities, and the exploitation of frequencies up to 80 MHz for use on shallow sites in dermatological and ophthalmic work (where enhanced spatial resolution is required, but the increased absorption at these frequencies is not debilitating). Non-imaging diagnostic methods have also developed, for example, in the use of ultrasound to investigate bone health and osteoporosis[10–15] through measurement of sound speed and attenuation.

The requirements of military sonar have driven many of the oceanic developments in acoustic monitoring and measurement. The end of the Cold War prompted a move away from the study of low frequency acoustics (a few kHz and below) in deep waters that had been used, for example, to detect nuclear submarines beneath the polar icecaps. In the last decade, military engagements have tended to occur in

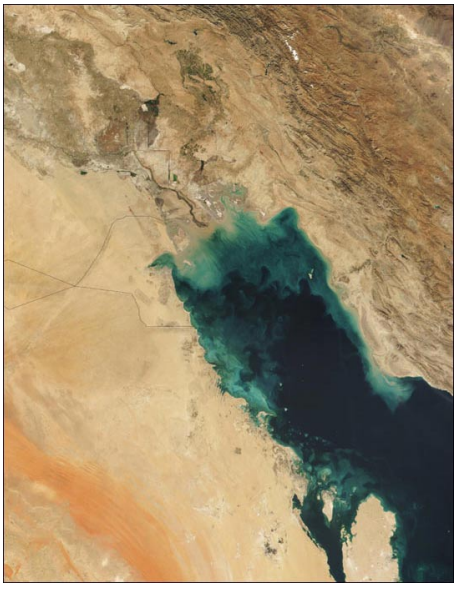

Fig. 1. True-colour satellite image (from the Moderate Resolution Imaging Spectroradiometer MODIS carried by NASA) of sediment carried by the Tigris and Euphrates Rivers. The sediment-laden waters of the Persian Gulf (November 1, 2001) appear light brown where they enter the northern end of the Persian Gulf and then gradually dissipate into turquoise swirls as they drift southward (Image courtesy Jacques Descloitres, MODIS Land Rapid Response Team at NASA GSFC). The presence of sediment has for thousands of years been important for land fertility, and the possibility of monitoring this acoustically[181,182] developed in recent years out of studies of the detrimental effects of suspended sediment on sonar.[183–188]

shallower coastal waters, and research interests have reflected this. Exploration of higher acoustic frequencies[16] in these shallow waters promises many oceanographic spin-offs.[17–20] These include studies of zooplankton,[21] archaeological artefacts,[22] the seabed and suspended sediment (Fig. 1). However, throughout the relatively young discipline of *acoustical oceanography*,[17–20] and indeed whenever sound is passed through liquids, it is well known that if bubbles are present, their acoustical effects cannot be ignored, and will often dominate the problem. This observation will now be examined.

2.2. *Applications of bubble acoustics*

In liquids, the most acoustically active naturally-occurring entities are gas bubbles. Two images from the biomedical and oceanographic examples of Sec. 2.1 illustrate this. In both images, the strongest echoes are from bubbles.

In Fig. 2, where sonar has been used for geological surveying, the strong echoes indicate the presence of shallow gas beneath the sea bed. However, in contrast to applications discussed later, this use of acoustics provides no direct quantitative information about the bubble population (such as the size distribution of bubbles

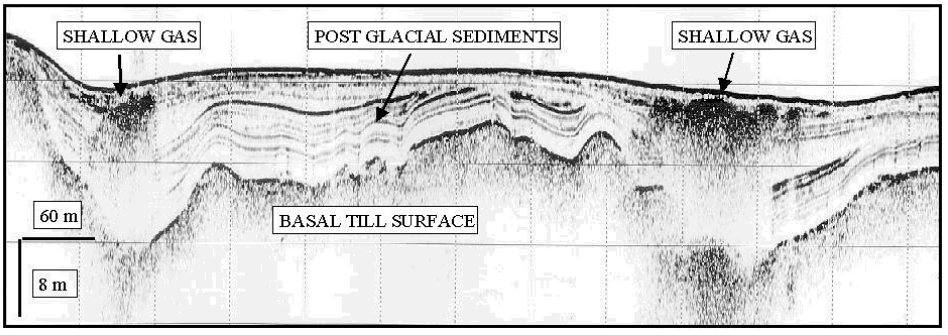

Fig. 2. A chirp sonar image, showing a cross-section of the seabed (maximum penetration approximately 20 m) in Strangford Lough, Northern Ireland. The dark line, which is usually 8–10 m from the top of the frame, indicates the sea floor. Hence, the labelled features are beneath the seabed. These include shallow gas deposits in the underwater sediment. The sonar cannot penetrate these as the majority of the sound is scattered from the gas bubbles. As a result, very little information is obtained from beneath the gas layers. Reproduced by permission of Southampton Oceanography Centre (J. S. Lenham, J. K. Dix and J. Bull).

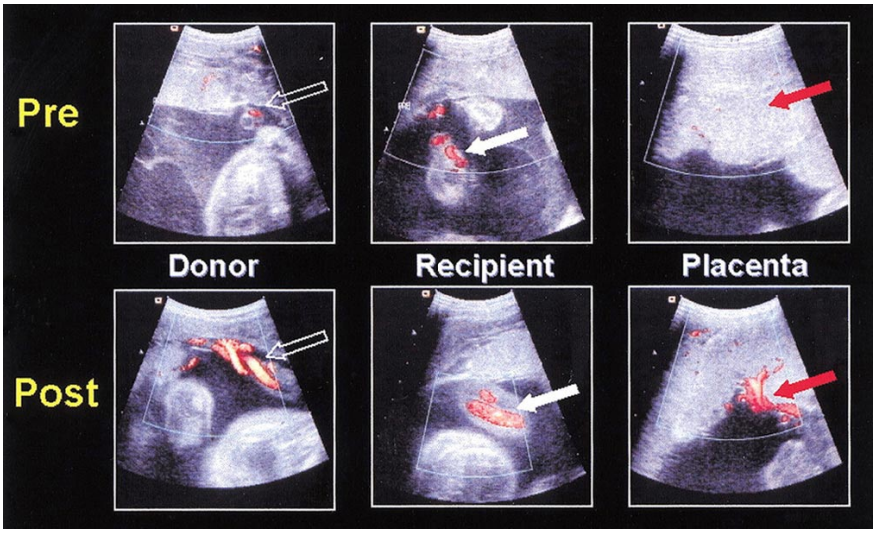

Fig. 3. The figure shows Power Doppler ultrasonic images before (top row) and after (bottom row) the injection of a commercial bubble-based UCA (SH U 508A) into the donor of a monochorionic twin pair. A threshold is preset: echo strengths from UCA exceed this, and are coloured red (although occasional returns which exceed the threshold in the absence of UCA are possible, as seen in the top row). In each case, the images show signal enhancements attributable to the contrast agent during maintenance of constant ultrasonic parameters. Left: Cross section through the first (Donor) twin's cord (arrow) before (top) and after (bottom) the administration of contrast agent. Middle column: cross section through the contralateral (Recipient) twin's cord (arrow) before (top) and after (bottom) interfoetal transfusion of contrast agent. Right: Placental appearance (arrow) before (top) and after (bottom) injection of contrast agent. Reproduced with permission from Denbow *et al.*[34]

present). In Fig. 2 the reflectivity of the bubbles is so strong that it hinders the penetration of sonar which might otherwise examine the seabed beneath the gas. Of course, most of the bubbles studied in *acoustical oceanography* are not trapped in sediment, but are free-floating in the water column. Their study is important to such environmentally significant processes as: coastal erosion and wave dynamics;[23–27] methane seeps;[28–30] and the fluxes between the ocean and atmosphere of momentum, energy and mass.[31] The top 2.5 metres of the ocean has a heat capacity equivalent to the entire atmosphere; and the flux[32] between atmosphere and ocean of carbon alone exceeds 10^9 tonnes/year.

Figure 3 however illustrates a far more sophisticated use of bubbles. Here, microscopic bubbles are injected into the body to act as ultrasonic contrast agents (UCAs).[1,33] Figure 3 illustrates current research in using the ultrasonic backscatter from bubble-based UCAs to save foetal lives affected by twin-twin transfusion syndrome. In 20% of cases where a single chorionic membrane surrounds both twins (i.e. "monochorionic" twins), the placenta provides vascular connections between the twins. Through these, blood can transfer from one foetus to another as a normal event.[34] However, in 15% of such cases, an imbalance occurs, leading to twin-twin transfusion syndrome. If left untreated, this has over 80% mortality (with complications present in some survivors). The acoustic impedance mismatch between blood and soft tissue is not great, and so the backscatter is not strong compared to the imaging of bone or gas bodies (e.g. in the gut). The ultrasonic imaging of blood flow can be greatly enhanced by UCAs. If UCA (here, based on microscopic bubbles) is injected into one twin, and subsequently appears in the bloodstream of the other twin, twin-twin transfusion has been diagnosed and the donor/recipient roles can be identified. If it were possible to discover which blood vessel in the placenta is responsible for the transfer, it could be sealed, saving both twins. Figure 3 demonstrates just such identification, and indeed recently a procedure has been completed where the blood vessel responsible for transfer was cauterised and sealed using high power ultrasound.[35] Other examples of the acoustic detection of *in vivo* bubbles[36] range from studies of decompression sickness[37,38] to knuckle cracking.[39–41]

Industry contains many examples of the need for reliable bubble detection, management and control systems.[2,42–44] In the petrochemical industry alone, for example, bubbles may be nucleated through the exsolution of gas which had dissolved into the crude oil in the high pressures at the well base, and which comes out of solution as the crude oil is being brought up to surface pressures. Knowledge of the bubble population is required to optimise harvesting, transportation and safety. Bubbles entrained during filling operations involving molten glass or polymer solutions,[45] or in the paint, food, detergent, cosmetics and pharmaceutical industries, may persist for long periods, degrading the product.[46] In the pottery industry, liquid "casting slip" is pumped from a settling tank, through overhead pipes and then into moulds for crockery, bathroom sinks, toilets, etc. These are then fired in a kiln to make the finished product. If bubbles are present in the slip, these expand during firing, and ruin the product, a problem which is only discovered after firing has taken place.

This means that the problem persists for many hours of production, wasting time, energy and materials (the fired pottery cannot be recycled). Before the invention of an acoustic system (Fig. 4), there was no way to monitor the presence of bubbles in the opaque slip.

Section 3 will discuss techniques for monitoring bubble populations for use in oceanography, biomedicine, industry and research. Sections 4 and 5 will speculate on the creatures with most experience of acoustics in bubbly waters, that is, cetaceans. We know almost nothing about whether they compensate for, or even exploit, the changes to acoustic propagation which bubbles impart to their environment. If they do exploit them, it may provide answers to current questions on enhancing sonar in shallow waters.

Given the exceptionally efficient coupling between bubbles and acoustic waves which Figs. 2 and 3 both demonstrate, it is perhaps not surprising that the potency of bubbles in acoustics is by no means restricted to diagnosis. In 1917, Lord Rayleigh identified the energetic bubble collapse known as "cavitation" as being the cause of the propeller failure which had been plaguing ships.[47] The ability of bubbles to process the materials which make them up and surround them will be discussed in Sec. 6.

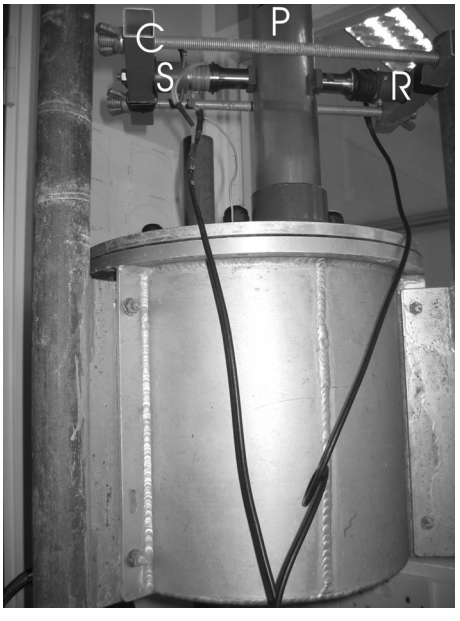

Fig. 4. The author (with students G. T. Yim and M. D. Simpson) invented an ultrasonic device for the detection of bubbles in the opaque liquid "casting slip" which is used by the pottery industry. The detector consists of ultrasonic source (S) and receiver (R) transducers mounted across from each other on the pipe (P). The system is held in place by a clamp (C) which is easily portable, and can be mounted at any position along the pipe, so allowing the operator to track down the source of the bubbles. For further details, including a video of the device in action, see the associated web page.[67]

3. Acoustic Bubbles in Diagnosis

Section 3.1 will discuss the detection of bubbles by the passive acoustic emissions (the "ringing") that they generate after entrainment. Typical examples include the "plink" of a dripping tap, the babbling of a brook or the crash of a breaking wave. In contrast, Sec. 3.2 will discuss the active acoustic techniques for determining the size distribution of bubbles present in a population. These operate by measuring the scattering, attenuation or modulation of a sound field which is projected at the bubble.

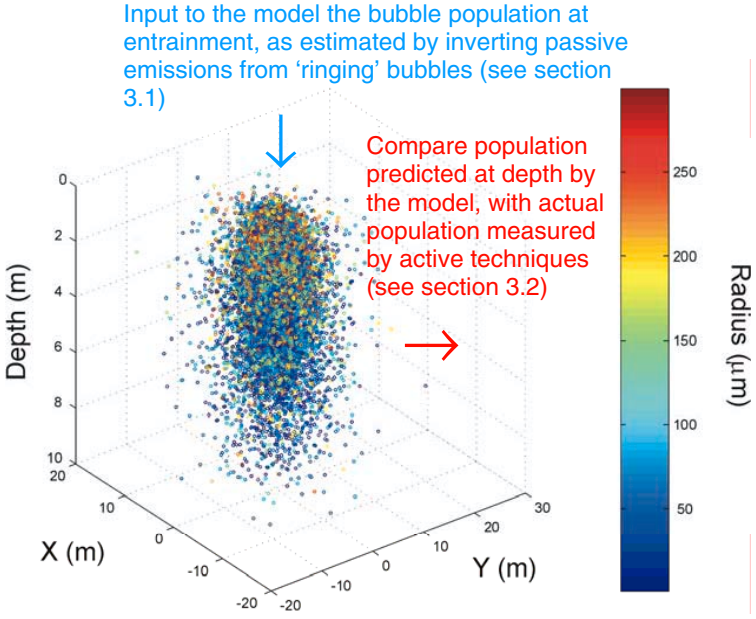

Fig. 5. A single frame from an animation illustrating the evolution of an oceanic bubble cloud, following its entrainment beneath a breaking wave (M. D. Simpson and T. G. Leighton). The air/sea interface is flat and at depth 0 m. The plot shows a 3D section of ocean measuring 40 m × 50 m × 10 m deep. The ocean itself is infinitely deep (although alternative models including seabeds are available via the associated web page[67]). This section of ocean is injected with a bubble population. This "ringing" population is based on measurements of the passive noise from breaking waves (as discussed in Sec. 3.1). The bubbles are initially placed in a cube measuring 0.5 m on one side, the top side being in the centre of the horizontal air-sea interface region shown. The population then evolves under the influence of buoyancy, turbulence, surface tension and hydrostatic pressure, and gas flux occurs as for example the bubbles dissolve.[189] (One process not yet included in this model is bubble coalescence and fragmentation.[57,66,190]) The frame shows the bubble cloud about 30 s after injection. The bubble size distribution is colour coded, and it is, for example, clear that whilst turbulence has dispersed the cloud spatially, both buoyancy and hydrostatic effects result in the tendency for small bubbles (blue) to occur at depth, with the larger (yellow/orange/red) bubbles tending to occur only close to the surface. The accuracy of such models were investigated[48] by comparing the predicted bubble population as a function of depth with the measurements[49] of active acoustic techniques, such as those described in Sec. 3.2. Each of the 64,000 bubbles in the simulation must represent approximately 10^4 bubbles in nature because of computational limitations. For further details see the associated web page.[67]

It should be noted[1,49] that the bubble populations measured by the passive techniques of Sec. 3.1 differ from the populations measured by the active techniques of Sec. 3.2. Passive emissions come only from those bubbles which are actively "ringing". This emission occurs only within the first few milliseconds after entrainment for most bubbles. Inversion of passive acoustic emissions will therefore estimate the population size distribution of "ringing" bubbles. Optical and active acoustic techniques actually measure the size distribution of a different bubble population, comprising not only the ringing bubbles, but also the silent bubbles which have ceased to ring, but which nevertheless persist in the water column. By comparing the results of active and passive measurements, it is possible to test dynamic models for the evolution of bubble clouds and so investigate the processes which occur beneath a breaking wave (such as turbulence, circulation, buoyancy, etc. see Fig. 5).[48,49] These processes convert the population initially produced by the breaking wave (the one measured by the passive acoustic technique) into the background population (as measured by the active acoustic technique). Section 3.1 will now outline the measurement of bubble populations from their "ringing".

3.1. *Natural oscillations of bubble pulsations in the small-amplitude linear limit*

After entrainment by breaking waves, waterfalls, injectors etc., the lightly-damped bubble pulsation emits into the far field an approximately exponentially decaying sinusoidal acoustic pressure signature at the natural frequency (Fig. 6(a)). Although bubbles are capable of undertaking the complete range of oscillations which the orders of spherical harmonic perturbation can describe,[2] with some exceptions,[50–53] it is the pulsation mode (zero order) which, as a monopole, contributes most effectively to the sound which propagates away from the bubble. The first measurements[54] of the size distributions of bubble populations in the natural world using these ringing emissions were made in 1985. The technique of inferring bubble radii in the natural world from the natural frequencies that they emit (Fig. 6(a)), has given rise to hundreds of studies,[17,20,55] from rainfall sensing[56,57] to industrial sparging[1,58–65] (the injection of gas under pressure through a liquid in order to facilitate processing). Development of this technique included the use of the Gabor Transform[57,66] and spectral methods for when entrainment rates are high.[1,55] A tutorial on such acoustic inversions is available via the web page.[67]

An interesting study was undertaken to show the extent to which we might invert the acoustic signal to obtain information on the bubble population and to demonstrate how useful this might be. The sound of the waterfall at Sadler's Mill, Romsey, UK (Fig. 7(a)) was recorded and its spectrum is shown by the solid line in Fig. 7(b). This spectrum was then used in an inversion calculation[68] to estimate the size distribution of "ringing" bubbles. This required an appropriate model for the emission from each bubble, and the left pane of Fig. 6(b) shows the model[1,55] used for the inversion, with the amplitude determined by the surface tension, the bubble

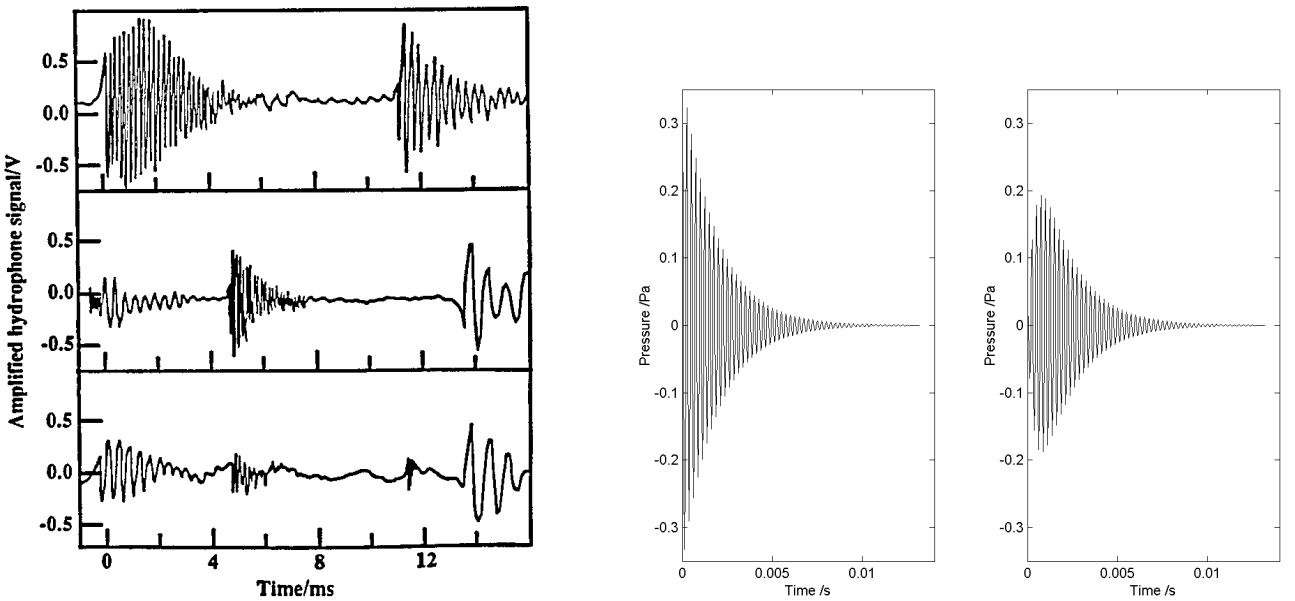

(a) (b)

Fig. 6. (a) Three selections from the hydrophone sound recording made at Kinder Scout in the Peak District (Derbyshire, UK). Each exponentially-decaying sinusoid indicates the bubble source as a lightly damped oscillator, the radius of which can be determined from the natural frequency. Here, the counting of bubbles is made simple because the low entrainment rate means there is little overlap between bubble signatures (from Leighton and Walton[54]). (b) Two idealised signatures for the same bubble, used in predicting the sound field of waterfalls on Earth and Titan. On the left is the simple exponential decay, the initial amplitude of which is determined by the acceleration due to gravity, the bubble depth and radius, and surface tension, with the decay rate calculated for damping through viscous, thermal and acoustic radiation losses. The modelled bubble was entrained at 10 cm depth, 3 m from the hydrophone (T. G. Leighton and P. R. White). This was the idealised pulse used in the first-order calculation of the spectrum of a "waterfall" on Titan.[68] The pulse on the right has in addition to these features a ring-up; otherwise the parameters are identical. It was this form of the pulse that was used in the second-order calculation[1] for Earth and Titan.

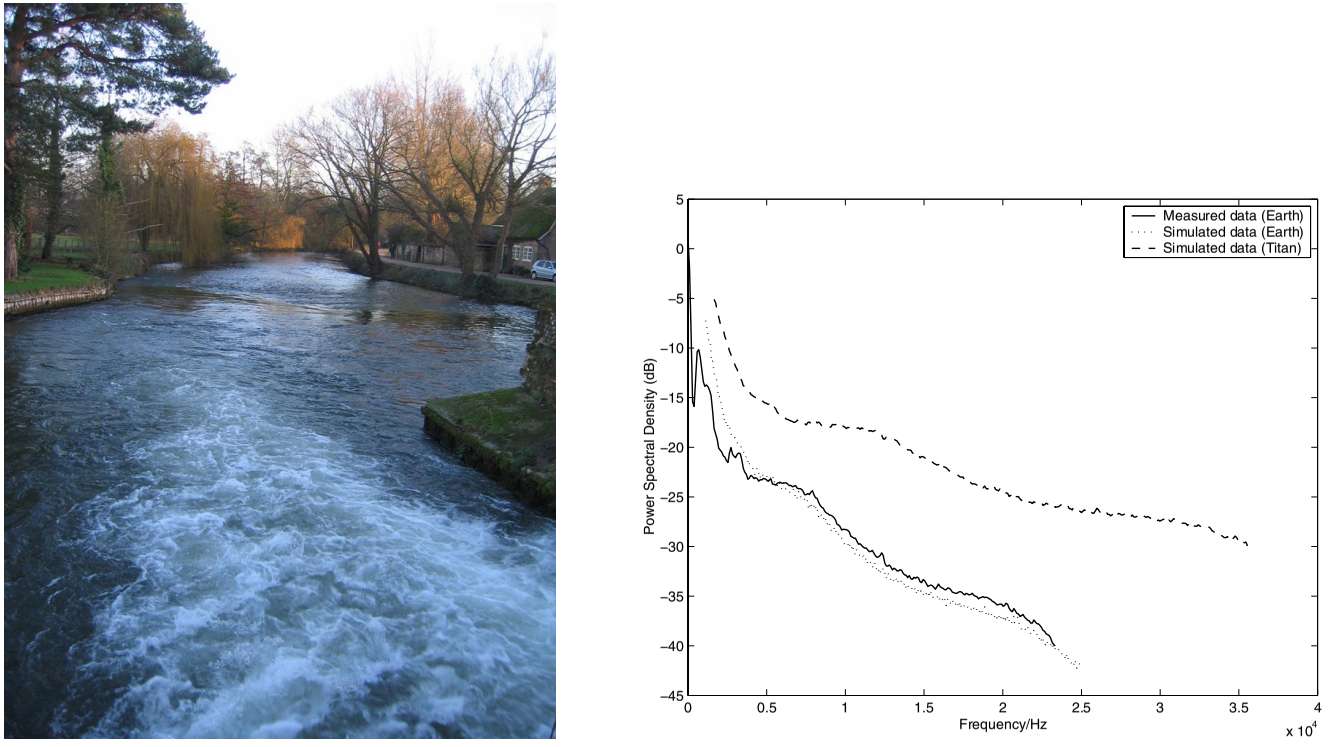

(a) (b)

Fig. 7. Underwater sound recordings at (a) Sadler's Mill, Romsey, Hampshire, UK, have a spectrum as indicated by the solid line in (b). These sounds were inverted to obtain the bubble size distribution which was being created at Sadler's Mill. Inputting this population into the model, with the parameters of Earth, the spectrum of the Sadler's Mill waterfall is recreated (part (b), dotted line). Similarly, if the same bubble population were to be entrained by a methane-fall on Titan, the model predicts the spectrum of the resulting sound (part (b), dashed line). All dB levels are relative to a common arbitrary reference. Further details, including a tutorial on inverting sounds of waterfalls to find the bubble population and details of the Titan study (including the sounds of water- and methane-falls, and splashdowns) can be accessed via the associated web page.[67] (Figure by T. G. Leighton and P. R. White).

size and the depth at which it is entrained.[68] The right pane of Fig. 6(b) shows the result of an improved model which is currently being applied to the same problem.[1]

Having obtained an estimate of the population of "ringing" bubbles, this population was then entered as input into the model, with appropriate parameters for Earth, in an attempt to reconstruct the sound of the Sadler's Mill waterfall artificially (Fig. 7(b), dotted line). Having therefore some confidence in the technique (based on the similarity of these two spectra), assume that there is a methane-fall on Titan (the largest moon of Saturn) which entrains the same bubble size distribution as was found at Sadler's Mill (Fig. 8). If this is the case, then by using this population as input into the model and using physical parameters appropriate for Titan, it is possible to predict the spectrum of the resulting sound (Fig. 7(b), dashed line). Recordings of these sounds and similar predictions of possible splashdown sounds can be accessed via the web page.[67]

The purpose of this exercise is to demonstrate the opportunities which acoustic measurements offer for space exploration. The signal has low bandwidth, the hardware is rugged, and typically has low mass, low cost and low power requirements. Given the myriad uses for diagnosis by bubble-generated sound on Earth, from rainfall sensing to investigating atmosphere/ocean mass flux, this exercise illustrates that the use of sound in general as an extraterrestrial diagnostic presents intriguing possibilities. Titan will in fact be visited by the *Cassini–Huygens* mission in early 2005 (Fig. 8), and *Huygens* contains an on-board microphone.

Fig. 8. Artist's impression of the *Huygens* probe parachuting through Titan's atmosphere, having previously detached from the *Cassini* vehicle (seen in the upper left of the image). With a 93 K surface temperature, Titan may possess the methane/ethane equivalent of the Earth's water cycle, and the picture shows the resulting methane-fall and clouds (Painting by D. Seal; Credit: NASA/JPL/Caltech).

The passive emissions and resonances from bubbles appear to be ubiquitous because entrainment on Earth (by injection, pouring, wave breaking, etc.) typically generates bubbles having radii ranging from millimetres to microns. These provide pulsation natural frequencies in the frequency range of at least $\sim$ 1–500 kHz respectively (with commensurate quality factors of roughly 30 to 5). This radius-to-frequency mapping follows from a small-amplitude expansion of the nonlinear equation of motion[1] for the pulsations of a bubble about an equilibrium radius R_0. In the long wavelength limit ($kR_0 \leq 1$, where k is the acoustic wavenumber), the resulting damped circular natural frequency ω_b is:

$$\omega_\mathrm{b} = \frac{1}{R_0\sqrt{\rho_0}}\sqrt{3\kappa\left(p_0 - p_\mathrm{v} + \frac{2\sigma}{R_0}\right) - \frac{2\sigma}{R_0} + p_\mathrm{v} - \frac{4\eta^2}{\rho_0 R_0^2}}\,, \tag{1}$$

where p_0 is the static pressure in the liquid outside the bubble, η and ρ_0 are, respectively, the shear viscosity and mass density of the liquid (which is assumed to be incompressible), p_v is the vapour pressure, σ is the surface tension, and κ is the so-called polytropic index. This engineering term is not a fundamental quantity, but takes an intermediate value between γ (the ratio of the specific heat of the gas at constant pressure to that at constant volume) and unity, depending on whether the gas is behaving adiabatically, isothermally, or in some intermediate manner (such that the ideal gas relationship between the bubble volume (V) and its gas pressure (p_g) can vary between $p_\mathrm{g}V^\gamma = \text{constant}$ and $p_\mathrm{g}V^1 = \text{constant}$). Note that the use of a polytropic law only adjusts the way gas pressure changes in response to volume changes to account for heat flow between the gas and its surroundings. In most bubble acoustics models where it is used, κ takes a constant value over the oscillatory cycle and, when used in this way, can never describe net thermal damping during the oscillatory cycle of a bubble.[49] This will become apparent in the discussion of Fig. 18. However, the polytropic index does adjust the bubble stiffness for this heat flow.

In fact, Eq. (1) only includes damping due to shear viscosity η, which has the expected effect for a linear oscillator, such that the damped natural frequency is lower than the undamped one (obtained by setting $\eta = 0$). Equation (1) does not incorporate thermal or acoustic radiation losses, which require more sophisticated models.[1] Other corrections may be required to account for bubble-bubble interactions,[69,70] and models of the behaviour of bubble clouds show that these can possess natural frequencies much lower than those of the individual bubbles which make up the cloud.[71,72]

The assumption of free field conditions underpins the vast majority of the theory of bubble acoustics, including Eq. (1). However, almost all of the experimental realisations of bubble acoustics are not in the free field, and neglect of this can lead to errors in damping[73] of $\sim$100%. Usually, there is some acoustically free surface present (such as an atmosphere/liquid interface), which will generate reverberation. In addition, important classes of bubble oscillation also occur in tubes[74–77] (including ear canals and blood vessels),[78,79] in pipes,[80] and in a variety of other

geometries. Indeed, the generation of conical[81–84] bubbles led to applications in needle-free biomedical injectors.[85]

A simplified form of Eq. (1) was first derived by Minnaert[86] in 1933. He assumed adiabatic conditions ($\kappa = \gamma$) and no damping ($\eta = 0$). He also neglected the effects of vapour pressure and surface tension (i.e. $p_v = 0$ and $\sigma = 0$, respectively). In this limit Eq. (1) takes a particularly simple form, such that the undamped natural frequency ω_0 is inversely proportional to the equilibrium bubble radius R_0. For air bubbles in water under Earth surface conditions, this holds true for roughly $R_0 > \sim 15$ μm, such that $\omega_0 R_0 / 2\pi \approx 3$ Hz m. This means that the O(mm) bubbles entrained in brooks and streams produce an audio-frequency babble, whereas an O(MHz) biomedical sound field might resonate with a micron-sized bubble.

Minnaert verified this formula by determining the natural frequencies of bubbles injected into a water tank. This he did by comparing his recollections of their short-lived "plink" sounds with a standard tuning fork. The manner of this, the foundation experiment of linear bubble acoustics, is all the more remarkable when one considers that 12 years later, the first atomic bomb was exploded: "The pitch is determined by ear, taking for comparison the sound of a tuning-fork (C 263 VD about) and estimating fractions of half a tone .... The mean error appears to be of the order of a fifth of a tone. Moreover, the determination of the octave to which the sound belongs is very difficult for me, so that there remains an uncertitude of a factor of 2 in the absolute values of the vibration numbers."

Having discussed the natural frequencies of bubbles and the determination of their size through their ringing ("passive acoustic bubble spectroscopy"), the active equivalent will now be discussed.

3.2. *Active acoustic bubble detection, and the exploitation of nonlinearities*

When driven by an external sound field, it is through the pulsation mode discussed in Sec. 3.1 that bubbles undertake their acoustic resonance. This has been exploited in numerous systems for bubble detection[87] in industry, biomedicine and the oceans. At low amplitudes of pulsation, the driven bubble resembles a linear oscillator. However, under certain circumstances, notably when the void fractions (the volume proportion of free gas in a sample of bubbly water) are great and a signal must be propagated to distance, high driving amplitudes are required to overcome attenuation. Those bubbles exposed to driving fields of sufficiently high amplitude undergo nonlinear pulsation. Indeed, high void fractions often necessitate the exploitation of these nonlinearities, as will now be discussed.

Minnaert derived Eq. (1) by equating the maximum potential energy stored in the bubble gas during the oscillation, with the maximum kinetic energy invested in the surrounding liquid (which must move when the bubble pulsates), in the limit of simple harmonic oscillations. However, except in the steady state limit of the bubble's response to monochromatic forcing, the bubble is never[1] a truly

linear oscillator even at small amplitude. This is because the damping is frequency-dependent, and none of the resulting dissipative forces are proportional to a velocity term (e.g. rate of change of radius or volume). At finite driving amplitudes, its nonlinear and even chaotic characteristics are apparent.[88]

Indeed, the generation of nonlinear signals has been an invaluable tool in separating the strong echoes or attenuation resulting from pulsation resonance, from

Fig. 9. The first measurement of the bubble size distribution in the surf zone (at Hull, UK, using the technique of Fig. 12(c)). The acoustic detector is the small black circle clamped between the two smaller uprights. The wave measures approximately 10 ft tall. Taken from Leighton *et al.*[89]

(a) (b)

Fig. 10. Two video frames, taken a fraction of a second apart, showing (a) two of the author's students (S. D. Meers and M. D. Simpson) attempting to bolt sensors to a scaffolding rig which the team have just deployed at sea; (b) Mr Simpson's feet (Mr Meers is not visible). During the subsequent trial (of the techniques of Figs. 12(a) and 12(c)) the winds increased from the relatively calm conditions shown here to speeds in excess of 50 mph. Taken from Leighton *et al.*[49] For further details, and the video from which these frames are taken, see the associated web page.[67]

linear effects which simply result from strong scattering by much larger off-resonance bubbles. When the bubble population is very dense, such ambiguities hinder the use of the pulsation resonance as a method of determining the bubble size. Therefore, for example, in the first measurements[89] of the bubble size distribution in the surf zone (Fig. 9), a nonlinear combination-frequency technique had to be used. The surf zone is important for many applications, from deployment of landing craft to coastal erosion. It is often characterised by high void fractions, which dominate many of the acoustic issues there. It may therefore seem surprising that there are so few measurements of the bubble population there.[49] This is partly because the surf zone is prone to the large bubbles and high void fractions, which invalidate the theory underpinning most acoustical techniques for bubble monitoring. Also, noting that each cubic metre of water has a mass of roughly one tonne,

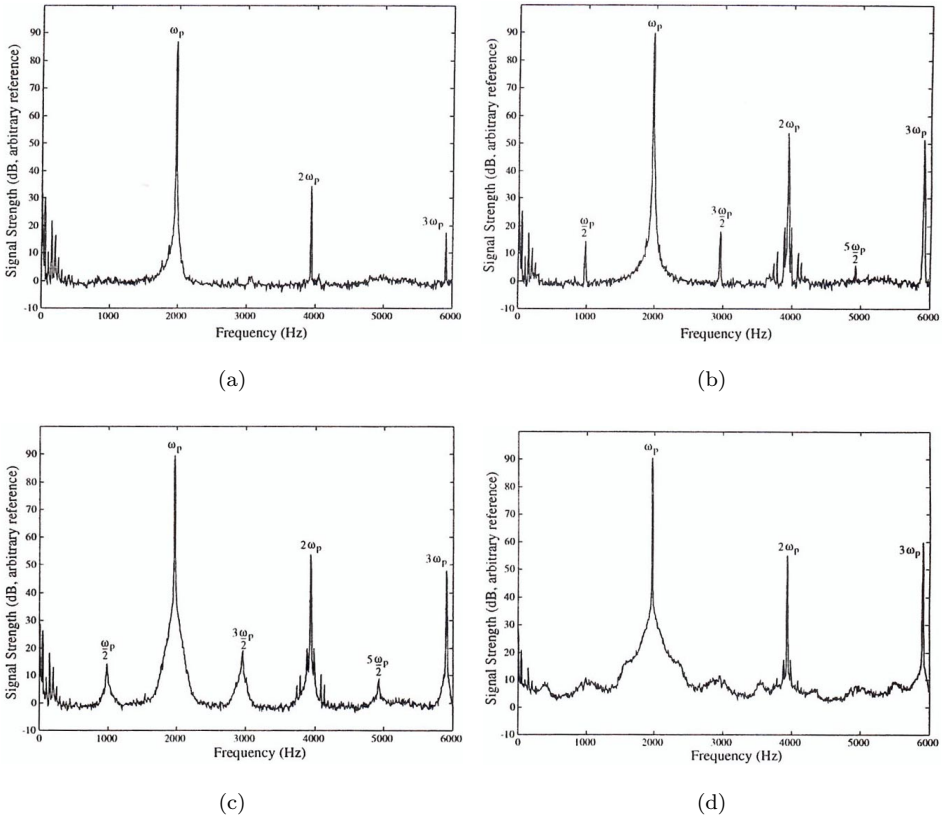

Fig. 11. Measured frequency response of the back scatter from a single bubble driven at its linear resonance frequency of $\omega_p = 1970$ Hz. The zero-to-peak acoustic pressure amplitude is (a) 110 Pa, (b) 150 Pa, (c) 180 Pa and (d) 260 Pa. As nonlinearities become apparent, the actual bubble resonance may of course drift from the low-amplitude linear value. Therefore, one would not necessarily expect the degree of nonlinearity to increase with driving pressure for a fixed insonification frequency (T. G. Leighton and A. D. Phelps).

it is in part because of the difficulties in deploying apparatus there and the need for rugged equipment (and staff[90] — see Fig. 10).

However, the bubble nonlinearity goes beyond a simple quadratic term which might generate these combination frequencies or second harmonics[91–96]: Subharmonics can be generated (Fig. 11); and the most precise[97–99] technique for the measurement of the size of a single bubble is through the generation of signals at $\omega_\mathrm{i} \pm \omega_\mathrm{p}/2$ when a bubble is insonified by a high-frequency imaging signal (at circular frequency ω_i) and a lower frequency "pump" signal (at circular frequency ω_p which is tuned to coincide with the bubble pulsation resonance). The mechanism responsible for this was found to be the generation of Faraday waves on the bubble walls (see Sec. 6).[100,101]

Other novel methods for characterisation of bubble clouds include the deployment of acoustoelectrochemical techniques at sea,[102] and the use of Higher-Order Statistics.[103–106] To counteract the ambiguities in any individual technique when employed in such challenging environments, multiple techniques may be used to counterbalance the limitations and ambiguities inherent in one technique.[97,98,107] When using any individual measurement method, and particularly when deploying a range of them, the invasiveness and interactions of techniques must be assessed.[108]

There are four classes into which one may group the so-called "active acoustic techniques for bubble spectroscopy". These are methods which insonify the bubble population with an external sound field in order to measure the bubble size distribution. They may be contrasted to the passive techniques of Sec. 3.1, which simply listen to the overall sound generated by bubble entrainment. These classes are shown in Fig. 12. A tutorial is available via the web page.[67] Parts (a)–(c) employ a pump signal, which is intended to drive the bubbles in pulsation. It is generically labelled ω_p in the figure, but may consist of a sequence of tones, a chirp or a pseudorandom sequence, and so on. For the technique of Fig. 12(a), the pump signal is transmitted between source and receiver (along a propagation path, or through backscatter, etc.). The bubble population is inferred from its effect on that signal (with respect to sound speed, attenuation or scatter; or the generation of harmonics or Doppler effects, etc.). In Fig. 12(b), a hollow vessel, which is characterised by resonant acoustic modes, is immersed and fills with bubbly water. The differences in the damping and resonant frequencies of those modes, compared to the bubble-free case, are related to the bubble population present within the volume.[109–111] In Fig. 12(c), the pump signal drives the bubbles into pulsation. This pulsation then modulates the scatter of a much higher frequency imaging signal (ω_i). The received signal then contains[100,101] sum and difference frequencies of ω_i and the frequencies present in the bubble oscillation (which may include harmonics and subharmonics of ω_p), that is, $\omega_\mathrm{i} \pm \omega_\mathrm{p}$, $\omega_\mathrm{i} \pm 2\omega_\mathrm{p}$, $\omega_\mathrm{i} \pm \omega_\mathrm{p}/2$, etc. In Fig. 12(d), both of the acoustic fields that are projected into bubbly water have frequencies (ω_1, ω_2) much higher than the bubble pulsation resonances, the latter being interpreted as the cause of signals[96] generated at $\omega_1 - \omega_2$. The deployment of apparatus for taking data using techniques (a) and (c) from Fig. 12 (for use in the study behind Fig. 5) is shown in Fig. 10.

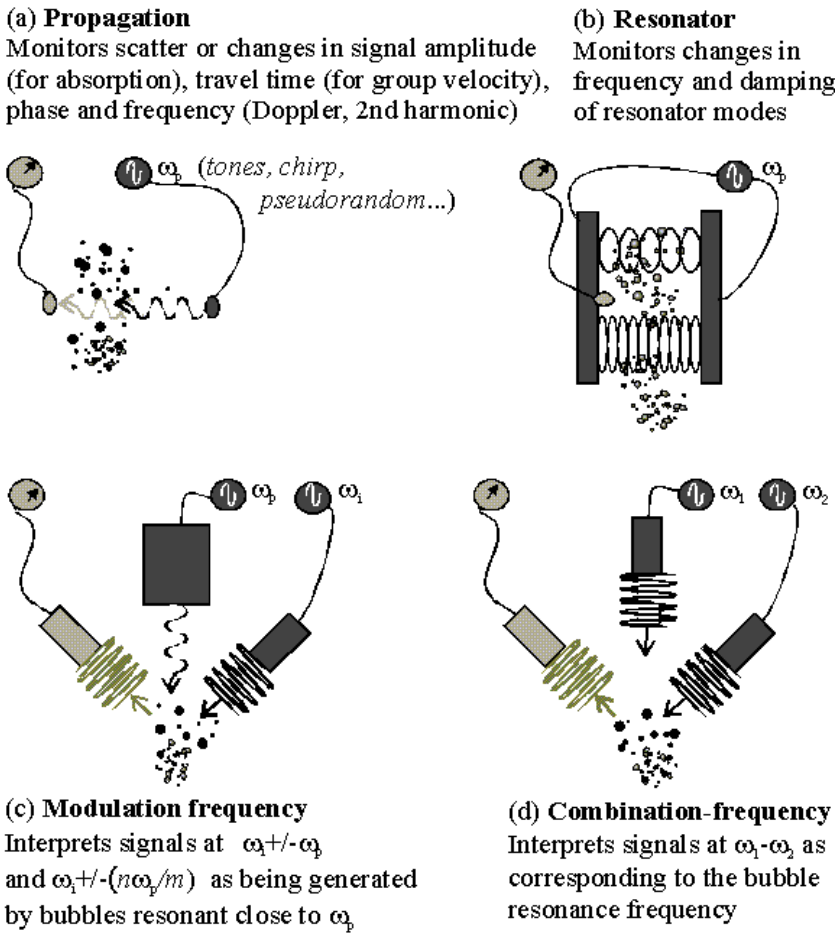

Fig. 12. The four main families of active acoustic techniques for obtaining the bubble size distribution. Transmitters and their waveforms are shown in dark grey; receivers and received waveforms are shown in light grey. The four families correspond to: (a) Propagation techniques; (b) Resonator method; (c) the bubble-mediated generation of modulation frequencies; and (d) the bubble-mediated generation of combination frequencies. Note that n and m correspond to non-zero integers. Most techniques are a manifestation or subset of these. For a tutorial on this, see the associated web page.[67]

Probably, the most popular technique for the active acoustic measurement of bubble populations is through monitoring the sound speed and attenuation of an acoustic signal as it propagates between two points (Fig. 12(a)). This has been done for both linear[112] and nonlinear[49] interpretations of the bubble dynamics. The effects of bubbles on the sound speed have been known for some time.[1,2,18,113] If the bubbles are driven in stiffness mode (the frequency of the imposed sound field is less than that of the bubble pulsation resonance, i.e. $\omega_\mathrm{p} < \omega_\mathrm{b}$), the presence of bubbles tends to reduce the sound speed in liquid. Even in the quasi-static

conditions attained at the lowest pump frequencies ($\omega_p \ll \omega_b$), there is a finite reduction in the sound speed. If bubbles in a population are driven by a sound field which has a pump frequency that is higher than any of the bubble pulsation resonances (i.e. $\omega_p > \omega_b$), they respond in an inertia-controlled manner. Here, they tend to increase the sound speed, the effect disappearing at the highest frequencies as the bubbles, now driven far off-resonance, undergo pulsations which are of very small amplitude.

The effect of bubbles on the sound speed and attenuation, and the boundary between linear and nonlinear interpretations of bubble acoustics, will be illustrated in Secs. 4 and 5, respectively. These explorations will encompass a natural situation about which we know very little, specifically the way cetaceans use sound in bubbly waters. Whilst the ideas are admittedly speculative, in the absence of data, such speculation is valid. This is in part because whales and dolphins (which, to a certain extent, live in an acoustic world) appear not to be impaired by bubbly water that would confound human sonar. Indeed, they even go to the trouble of generating artificial bubble fields in the water around them when they hunt. Hence, regardless of whether cetaceans actually do exploit the ideas presented here, the fact that the physics allows for the possibility indicates that there is the potential to enhance our own acoustic systems in bubbly water. This would benefit fields as diverse as biomedicine and human sonar, as will be shown below.

4. Cetacean Bubble Acoustics

The spectacular acoustic abilities of cetaceans are well known. Given the bubbly nature of the near-surface ocean layer, it is possible that we have much to learn from them regarding the exploitation of acoustics in bubbly water. It is therefore both frustrating and exciting that the verdict on all the material discussed in Secs. 4 and 5, is that the current paucity of measurements specifically to address the operation of cetacean sonar in bubbly water prevents us from proving or disproving any of these hypotheses. This is particularly so when we realise that cetaceans at times deliberately make their environment bubbly in order to facilitate their hunting.

Section 4 will speculate on one possible implication of the effects of bubbles on sound speed that were discussed at the end of Sec. 3. Specifically, this is that low frequencies tend to experience a reduced sound speed in bubbly water, and high frequencies propagate with an increased sound speed, with the effect disappearing at the highest frequencies. This led to a recent hypothesis[114] which might explain the mystery of the mechanism by which humpback whales (*Megaptera novaeangliae*) exploit bubble nets to catch fish.

It has been known for decades that humpback whales, either singly or in groups, sometimes dive deep and then release bubbles to form the walls of a cylinder, the interior of which is relatively bubble-free (Figs. 13(a) and 13(b)).[115] The prey are trapped within this cylinder, for reasons previously unknown, before the whales "lunge feed" on them from below (Fig. 13(c)). An acoustical explanation for why the

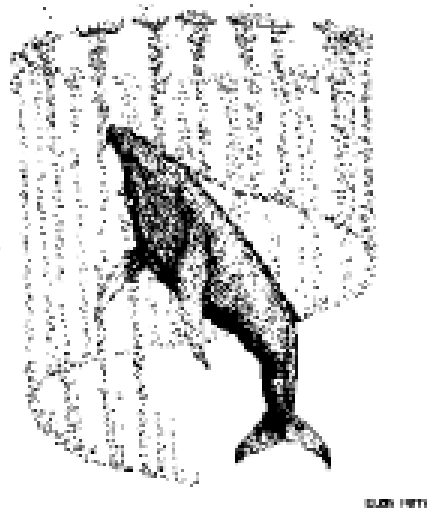

(a)

(b)

(c)

Fig. 13. (a) Schematic of a humpback whale creating a bubble net. A whale dives beneath a shoal of prey and slowly begins to spiral upwards, blowing bubbles as it does so, creating a hollow-cored cylindrical bubble net. The prey tend to congregate in the centre of the cylinder, which is relatively free of bubbles. Then the whale dives beneath the shoal, and swims up through the bubble-net with its mouth open to consume the prey ("lunge feeding"). Groups of whales may do this co-operatively (Image courtesy of Cetacea.org). (b) Aerial view of a humpback bubble net (Photograph by A. Brayton, reproduced from reference 191. The author has obtained permission from the publisher but has been unable to contact the photographer.) (c) Humpback whales lunge feeding (Image courtesy of L. Walker, http://www.groovedwhale.com).

prey are trapped has been proposed.[114] When the whales form such nets, they emit very loud, "trumpeting feeding calls", the available recordings[116] containing energy up to at least 4 kHz. A suitable void fraction profile would cause the wall of the cylinder to act as a waveguide. Figures 14(a) and 14(b) show how, with tangential[a] insonification, the mammals could generate a "wall of sound" around the net and a quiet region within it. If the fish approach the walls, they become startled by the intense sound (which may not only be subjectively loud, but also may affect the swim bladder, another resonant bubble system). The natural schooling response of fish to startling would, in the bubble net, be transformed from a survival response into one that aids the predator in feeding.

The ray model follows the frequency dependency described at the end of Sec. 3. Within a certain frequency range (estimated[1] to be 30–50 kHz on the untested assumption that the bubble size distribution in the net resembles that generated by breaking waves), the bubbles produce an increase in sound speed. The ray-tracing technique indicates that the net wall becomes outwardly-refracting and rays are no longer trapped within the cloud. A variety of ray behaviour is predicted,[1,114] from reflecting straight off the net to traversing it and the interior with barely any refraction (Fig. 14(c)).

Whilst, to date, there is no firm evidence of humpback whales exploiting such >30 kHz frequencies,[117] *odontoceti* are well known for emitting in excess of 100 kHz for echolocation.[118] However, the raypaths of Fig. 14 ignore scattering and attenuation, which tend to increase with frequency. Indeed, Sec. 5 explores how these two factors, omitted from the discussion so far, probably dominate the issue of whether *odontoceti* can echolocate in bubble nets.

First, however, to close this section on another speculative note, it may be that exploitation of the schooling of fish in response to startling using bubble acoustics is more widespread, if perhaps less elegant, than the scheme of Fig. 14(b). The filming associated with Byatt *et al.*[119] detailed bubble nets produced by dolphins[119] (Figs. 15(a)–15(d)). It also showed bubble plumes generated by gannets (Figs. 15(e)–15(g)) diving into a shoal of sardines which dolphins have herded to the sea surface. These plumes will no doubt complicate an underwater sound field already populated by the calls and bubble nets of dolphins, and the entrainment noise of the gannet bubble plumes, and could further stimulate the sardines

[a]Even if the whales do not create sufficiently directional beams and insonify tangentially, the bubble net might still function through its acoustical effects. The "wall of sound" effect in Fig. 14(b) is generated from those rays which impact the wall at low grazing angles. Those rays which never impact the wall do not contribute to the "wall of sound". If rays of higher grazing angle impact the net, they may cross into the net interior, though their amplitudes would be reduced by the bubble scattering, and attenuation alone would generate a quieter region in the centre of the net. This article gives a necessarily brief summary of the phenomena. Interested readers should see the references and website for discussions of the numerous qualifying features, including the justification for use of ray representation, the speculation on the beamwidth and the possibility of three-dimensional, collective and nonlinear effects (including parametric sonar).

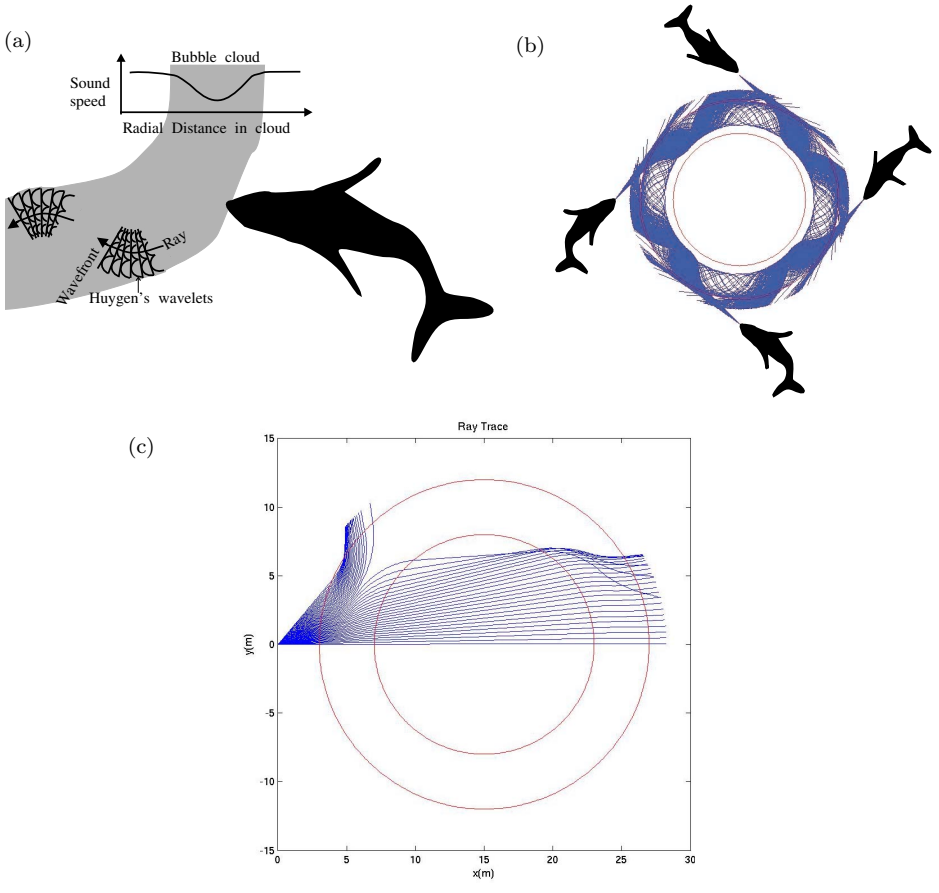

Fig. 14. (a) Schematic of a whale insonifying a bubble-net (plan view), illustrating the sound speed profile in the cloud and, by Huygen's construction, sample ray paths. The sound speed profile assumes void fractions are greatest in the mid-line of the net wall, and assumes that the bubbles pulsate in stiffness mode. Hence, the closer a Huygens wavelet is to the mid-line, the smaller the radius of the semicircle it forward-plots in a given time. Rays tend to refract towards the mid-line. (b) Plan view of four whales insonifying an annular bubble net (see (c) for its dimensions). Here, the bubbles are driven in stiffness-controlled mode such that the sound speed decreases linearly from 1500 m/s at the walls (i.e. the sound speed in bubble-free water), to 750 m/s at the cloud midline (corresponding to a void fraction there of ∼0.01%). The rays are coloured blue, and the locations of the inner and outer walls of the net are shown in red. Computed ray paths, where each whale launches 281 rays with an angular extent of 10°, refract as in (a). The rays gradually leak out, although some rays can propagate around the entire circumference. Plotting of a raypath is terminated when it is in isovelocity water and on a straight-line course which will not intersect the cloud. This refers to rays whose launch angles are such that they never intersect the net; and to rays which, having entered the net and undertaken two or more traverses of the mid-line, leave it. (c) Example ray paths computed for a cloud where the bubbles are driven in inertia-controlled mode such that the sound speed increases linearly from 1500 m/s at the walls to 2250 m/s at the cloud midline. The locations of the inner and outer walls of the net are shown by the two concentric circles. For this simulation, however, the single source has a 45° beamwidth in order to illustrate the variety of ray bending that is possible (a 10° beam, as used in (b), tends to cause all rays follow a similar path, either traversing the net or refracting out of it, depending on the angle with which it intercepts the outer wall of the net). (Figures from T. G. Leighton, S. D. Richards and P. R. White).[114] For further details see the associated web page.[67]

to school. Gannets, dolphins, sharks and whales, etc. (Fig. 15(h)) all benefit from this, although to what extent this is intentional is unknown.

Bubble clouds could have uses underwater, from the protection of breeding rights in cetaceans to noise in vessel wakes. Simple bubble screens have already been exploited to protect fish stocks from the noise of piling and other human

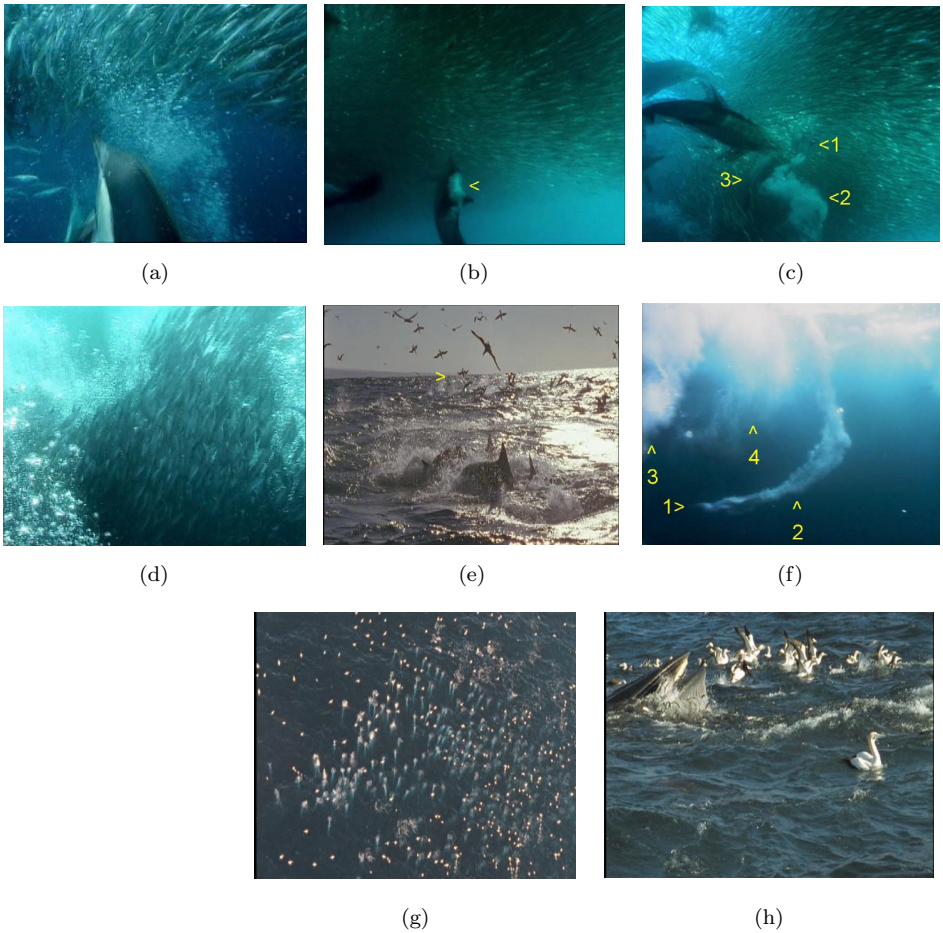

(a) (b) (c)

(d) (e) (f)

(g) (h)

Fig. 15. (a) Common dolphins herd sardines with bubble nets. (b) Swimming beneath a school of sardines, a dolphin starts to release a cloud of bubbles (arrowed) from its blowhole. A moment later (c) the dolphin (1) swims on, leaving behind the expanding cloud (2). Other dolphins (incl. 3) enter the frame. (d) The sardines school within a surrounding wall of bubbles that they are reluctant to cross, whilst (e) gannets dive into the sardine shoal to feed, folding their wings just before entry (arrowed). Dolphins are visible in the foreground. (f) On diving, a gannet (1) entrains a bubble plume (2). Plumes a few seconds old (3, with an older 4) have spread. (g) An aerial view shows hundreds of tight bubble plumes beneath airborne gannets. Imagine a torpedo trying to negotiate a field of gannet countermeasures! (h) A Bryde's Whale joins the feed. It surfaces with open mouth, which it then closes, sardines spilling from it. Images courtesy of The Blue Planet (BBC). See Byatt *et al.*[119] For further details see the associated web page.[67]

activity,[114,120,121] although the understanding of the associated acoustics has been very limited. The following section takes the speculation on the interaction between marine mammals and bubble clouds further, into an examination of the possible role that bubble nonlinearities might play in this.

5. Linearity and Nonlinearity in Acoustic Scattering from Bubbles

The linear theory for acoustic propagation through bubbly water has proved to be immensely successful, with the original paper[122] being cited over 100 times. However, bubble pulsations are inherently nonlinear[1] (Fig. 16), and the propagation of high amplitude fields in bubbly water needs to account for this.[49]

Moreover, development of time-dependent and nonlinear methods may provide solution to current problems, for example, in the exploitation of contrast agents in biomedicine and in the development of new techniques for the detection of mines in bubbly water.[1,123,124]

The importance of mine-hunting in modern warfare is very great. Since the start of the Cold War, at least 14 U.S. ships have been damaged by mines, with

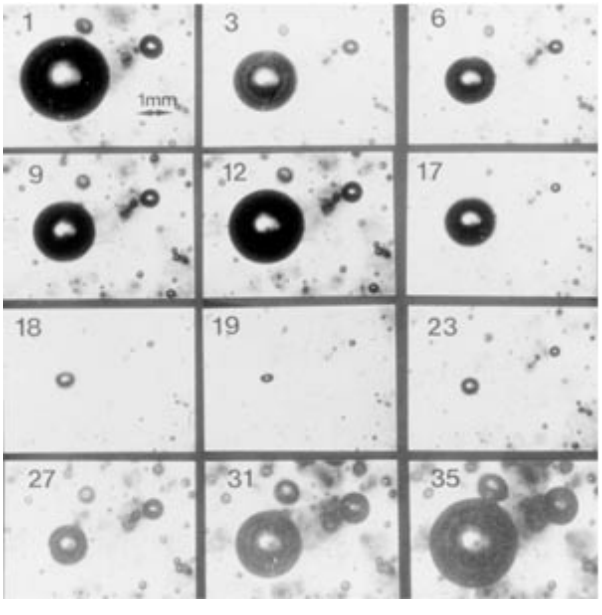

Fig. 16. Nonlinear bubble pulsation in 100 Hz pressure field generated to the oscillation of a liquid column and filmed at 2,000 frames per second. A selection of frames from the sequence of 35 consecutive frames show 1 period of the motion of stable air bubble oscillating in glycerol under a static pressure of 600 Pa and oscillating pressure of 3900 Pa. The bubble contracts from maximum size in frame 1 to a minimum in frame 6, then expands to a second maximum (frame 12). It then collapses to a second minimum (as frame 19) before expanding to the initial size. This cycle then repeats. The second collapse is gradual up to frame 17, but then becomes very rapid. (Figure from Leighton *et al.*[192]).

some sinking. Mine clearance techniques include attempting to cause detonation by presenting the mine with a signal resembling that which its target would produce. To resist such attempts, mines of considerable sophistication are being developed, which respond to the pressure, magnetic, underwater electric potential and acoustic signatures of vessels (often in combination). However, mines have a long operational lifetime, and simple contact devices produced decades earlier (which can be readily purchased) are inexpensive and effective (Fig. 17(a)). In 1988, a simple contact mine costing $1,500 (an Iranian SADAF-02) almost sank the *Samuel B. Roberts* (FFG-58), causing nearly $96 million of damage. During the first Gulf War, Iraq laid 1242 mines and even though many were nonfunctional or ineffectively laid, three mines seriously damaged two U.S. warships, *Princeton* (CG-59) and *Tripoli* (Fig. 17(b)). These mines were laid in water 20–50 m deep.

In very shallow waters, appropriate mines might be very successfully hidden by exploiting the bubble fields. There, the presence of mines presents a hazard to landing craft, such that even without detonating, the mine can seriously interfere with marine activity, which must be conducted cautiously. Sonar attempts to detect mines in very shallow water can fail because the returned sonar signal can be dominated by the scatter from the wave-generated bubble clouds in the vicinity of the mine. Time-dependent[125] and nonlinear[49] techniques might enhance scatter from a mine and suppress that from the bubbles, aiding detection,[1] as the behaviour of dolphins may indicate.

Figure 15 indicates that, like humpback whales, some dolphins also use bubble clouds to herd fish during feeding. However, linear theory would suggest

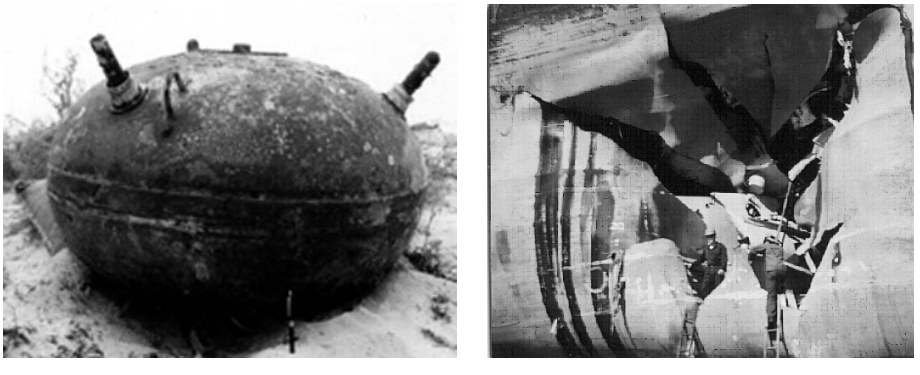

(a) (b)

Fig. 17. (a) An LUGM-145 (available for $1900). It carries a 660 kg charge, is based on a pre-First World War design, and is moored on a chain or drifts on the surface and is set off by contact with a ship. Modern mines are triggered by a ship's magnetic, acoustic or pressure signature (or combination of the above) so that they cannot readily be cleared by dummy contact methods. (b) Around $5 million of damage was caused to the *USS Tripoli* (LPH-10) after it struck an LUGM-145 moored contact mine during operation Desert Storm (Dstl were consulted before reproduction of this image).

that echolocation would be impossible in such an environment. For the bubble population assumed in plotting Fig. 14, linear theory indicates that, whilst acoustic attenuation at 4 kHz (the higher end of the frequency range used in the feeding calls) is ∼6 dB/m, it increases substantially with frequency, exceeding 200 dB/m at the higher frequencies used by *odontoceti* in echolocation (>100 kHz). This raises the interesting dilemma. When they generate bubble clouds to hunt, are dolphins really nullifying their most spectacular sensory apparatus, in an environment so visually complex that successful echolocation would be very beneficial? Or have the dolphins adapted their sonar to work in this environment?

To investigate this, note that the above attenuations were calculated using linear theories of bubble acoustics, the standard method to date.[122] However, plots of the applied pressure P against bubble volume V show that, if the bubbles in the cloud behave nonlinearly, the results can be very different.

First, consider a monodisperse bubble population (i.e. all bubbles have the same equilibrium radius) pulsating in the linear steady-state (Fig. 18). If the propagation were linear and lossless, the graphs of applied pressure (P) against bubble volume (V) would take the form of straight lines, the location of the bubble wall being plotted by the translation of the point of interest up and down these lines at the driving frequency (Fig. 18, top row). Since a positive applied pressure compresses a bubble in the stiffness-controlled regime, here $dP/dV < 0$ (Fig. 18, Row 1, right).

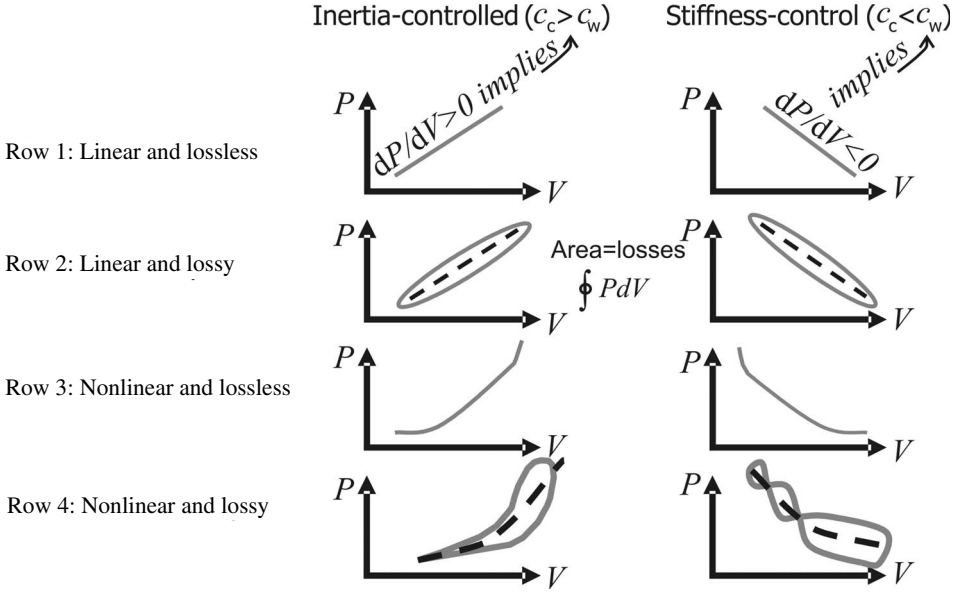

Fig. 18. Schematics of applied pressure versus steady-state bubble volume oscillations. The left column shows the result for the inertia-controlled regime ($\omega_p > \omega_b$) and the right column corresponds to the stiffness controlled regime ($\omega_p < \omega_b$). The four rows correspond to conditions which are (from top downwards): linear and lossless; linear and lossy; nonlinear and lossless; nonlinear and lossy.

However since a phase change of π radians occurs across the resonance, the opposite is true in the inertia-controlled regime ($dP/dV > 0$, Fig. 18, Row 1, left).

The behaviour of the top row of Fig. 18 reflects the trend indicated at the end of Sec. 3, that sound speed in bubbly water (c_c) is increased in the inertia-controlled regime and decreased under stiffness-control. This can be shown[49] from the fact that, in an infinite body of either water or gas that contains no dissipation, sound speeds (c_w and c_g respectively) may be defined:

$$c_\zeta^2 = \frac{B_\zeta}{\rho_\zeta} = \left(\frac{\partial P(\rho, S)}{\partial \rho} \right)_\zeta \quad (\zeta = \mathrm{w}, \mathrm{g}) \tag{2}$$

where S is the entropy, B_ζ is the bulk modulus and ρ_ζ the mass density, and the subscript ζ refers to application to bubble-free water (w) or gas (g) throughout Eq. (2). Obviously, a bubble which is driven in the inertia-controlled regime will be expanding during the compressive half-cycle of the driving pulse, which contributes a component increase in volume to the bubbly water during compression. The sign of $dP/dV > 0$ implies, through (2), that inertia-controlled bubbles will increase the sound speed in bubbly water (c_c) above that found in bubble-free water (c_w). In the stiffness-controlled mode, the bubble will compress to a greater extent than the volume of water it replaces during this compressive half-cycle. Hence through Eq. (2), the usual phase change which occurs across resonance means that, in the stiffness-controlled regime, $dP/dV < 0$. This in turn changes the sign of the contribution made by the bubbles to the sound speed in the mixture,[49] and $c_c < c_w$. If the bubble population contains a range of equilibrium radii, an appropriate summation is required.[49]

If conditions are linear and lossy (Fig. 18, Row 2), each acoustic cycle in the steady-state must map out a finite area which is equal to the energy loss per cycle from the First Law of Thermodynamics. The sound speed can be estimated using the dP/dV gradient of the spine of the loop (shown in Fig. 18 as a dashed line). Assume that the gas is perfect. Its internal energy U is a state function, such that whenever an orbit crosses its previous path, at both moments represented by the intersection, the value of U is the same. More specifically, consider that:

$$dU = đQ + đW = đQ - PdV \tag{3}$$

where the notation indicates that both the incremental heat supplied to the bubble ($đQ$) and the work done on the bubble ($đW$) are not exact differentials, whilst dU is.

Because Fig. 18 (and later, Fig. 19) use the applied acoustic pressure $P(t)$, the area mapped out by any loop represents the energy subtracted from the acoustic wave by the bubble in the time interval corresponding to the perimeter of the loop. This is because the bubble dynamics (such as used here) may be interpreted simply as a statement of the equality between that pressure difference (Δp) which is uniform across the entire bubble wall, and a summation of other terms.[1,49] These terms[2] relate to the pressure within the gas/vapour mixture inside the bubble (p_i), surface tension pressures (p_σ) and the dynamic terms resulting from the motion of

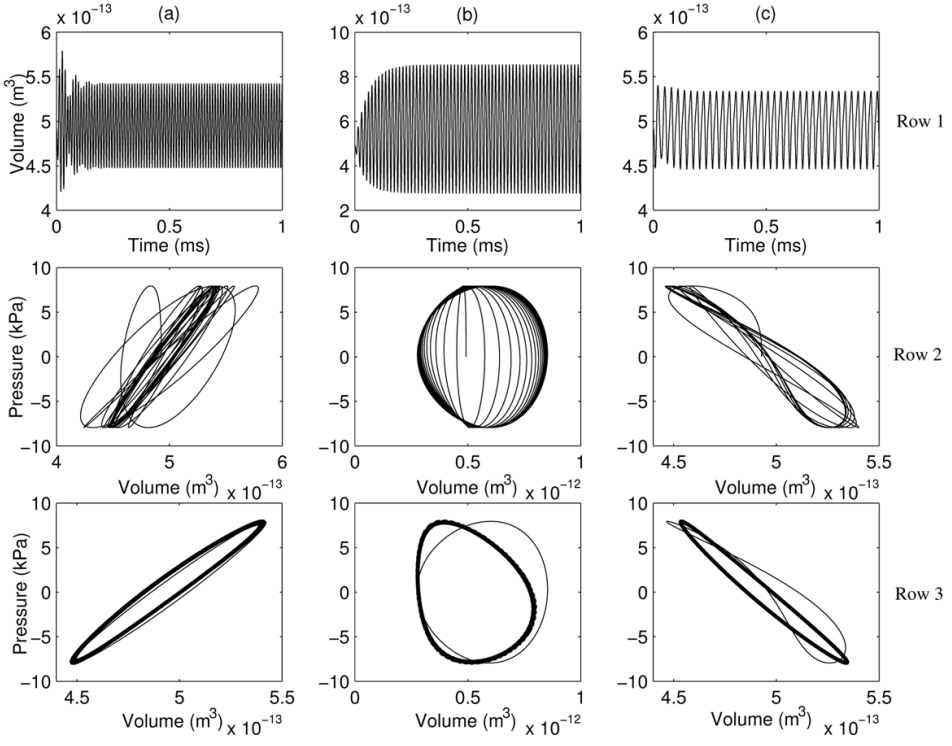

Fig. 19. Bubble responses for a 49 μm radius bubble insonified by a semi-infinite pulse starting at $t = 0$ with an amplitude of 7.95 kPa at (a) 84.2 kHz, (b) 65.7 kHz and (c) 31.5 kHz. The top graph in each case shows the volume time history calculated using the a nonlinear equation of motion for a bubble with appropriate damping.[49] The middle graph in each case shows the corresponding pressure-volume curve (applied pressure versus bubble volume). The darker area in each P–V curve shows the steady state regime, where the successive loci overlap each other. Nonlinear components will cause crossovers in a loop (as in part (c) where a second harmonic arises from driving the bubble close to half resonance frequency). In calculating the energy dissipated by the bubble through integration of such pressure-volume maps, the areas of the clockwise loops will be subtracted from those of the anticlockwise. The bottom row superimposes the steady-state loops of the middle row (thin line) with the corresponding linear solution using the steady-state linear formulation (thick line). After Leighton *et al.*[49]

the liquid required when the bubble wall is displaced, which will here be termed p_{dyn}. Thus,

$$\Delta p = p_{\mathrm{i}} - p_{\mathrm{dyn}} - p_{\sigma}\,. \tag{4}$$

The energy E_{loop} subtracted from the sound field by the pulsating bubble in each circuit of a loop is given by

$$E_{\mathrm{loop}} = -\oint p_{\mathrm{i}} dV + \oint p_{\mathrm{dyn}} dV + \oint p_{\sigma} dV \tag{5}$$

(noting that the details of the chemistry on the bubble wall may make the final integral non-zero). However, Δp equals the spatial average over the bubble wall of the blocked pressure $\langle p_{\mathrm{blocked}} \rangle$, which in the long-wavelength limit equals the

applied acoustic pressure $P(t)$ that would be present at the bubble centre were the bubble not present. Substituting Eq. (4) into Eq. (5) therefore shows that the area mapped in a loop in the applied pressure-volume plane is the energy subtracted from the acoustic wave in the time interval corresponding to that loop:

$$E_{\text{loop}} = -\oint \Delta p dV = -\oint \langle p_{\text{blocked}} \rangle dV \approx -\oint P dV \quad (kR \ll 1)\,. \tag{6}$$

Therefore, the rate at which the acoustic field does work on the bubble can be found by integrating the area in the pressure-volume plane enclosed by the loops formed by the intersections described above, and dividing the energy so obtained by the time interval taken to map out that loop. In this way, the rate at which the bubble subtracts energy from the driving acoustic field can be calculated.

Traditionally in bubble acoustics, researchers have found greatest imprecision and difficulty in defining a sound speed near resonance. Row 2 of Fig. 18 illustrates how this will coincide with conditions where not only is the area mapped out very large, but the characteristic gradient of dP/dV is very difficult to identify (in keeping with known through-resonance behaviour of sound speed in monodisperse populations[113]). (This will be explicitly demonstrated in the later discussion of Fig. 19).

If conditions are nonlinear and lossless (Fig. 18, Row 3), in steady-state the P–V plots must encompass zero area, but they will depart from straight-lines (e.g. because the degree of compression cannot scale indefinitely). The gradient dP/dV varies throughout the acoustic cycle in a manner familiar from nonlinear acoustic propagation, and this can appropriately describe nonlinear propagation and the associated waveform distortion in the usual manner.[126]

If conditions are nonlinear and lossy (Fig. 18, Row 4), finite areas are mapped out, and whilst the characteristic spines may present significant challenges, nonlinear propagation may again be identified (the example on the right of Fig. 18, Row 4 illustrates a strong third harmonic, where the steady-state volume pulsation undertakes three cycles for each period of the driving field).

This scheme can now be used to interpret Fig. 19, which uses a nonlinear model[49] to predict the response of a single air bubble (of equilibrium radius 49 μm) in water, subjected to a semi-infinite sinusoidal driving pulse (starting at $t = 0$). Under linear Earth surface conditions, this bubble has a resonance of 65.7 kHz. The left column, (a), corresponds to insonification at 84.2 kHz, a frequency greater than resonance, that is, the inertia-controlled regime. The middle column, (b), corresponds roughly to a bubble at resonance (65.7 kHz). The column on the right, (c), shows insonification at 31.5 kHz, a frequency less than resonance (i.e. the stiffness-controlled regime).

Figure 19, Row 1 shows the volume time history of the bubble, as predicted by a nonlinear model.[49] Row 2 plots the same data in the plane of the applied pressure versus bubble volume. The locus of this plot consists of a single point until the onset of insonification. From this moment on, the locus describes orbits until

reaching steady-state, after which it repeatedly maps out a given orbit. The time-dependent rate at which each bubble in the population subtracts energy from the driving acoustic field can be calculated in the manner described for Fig. 18, with steady state being achieved as $t \to \infty$ (Fig. 19, Row 2).

Of particular interest is Row 3 of Fig. 19, which superimposes the steady-state nonlinear loops of the middle row (thin line) with the corresponding linear steady-state solution (thick line). At frequencies much greater than or less than resonance (not shown), both models predict loci indistinguishable from straight lines (dissipation and nonlinearities being negligible at such extremes, the area mapped out by each loop is very small). The gradients of these lines have opposite signs, in keeping with the phase change of π radians which takes place between the stiffness- and inertia-controlled regimes.

Closer to resonance, increasing dissipation imparts finite areas to the loops, and the sound speed must be inferred from the spine of the loop. While in some cases the nonlinear model would impart a similar spine to its loop as would that of linear theory (Fig. 19(a), Row 3), closer to resonance identification of the optimum spine becomes more difficult (Fig. 19(b), Row 3; note that the conditions for resonance in the nonlinear and linear models are slightly different). The increasing dissipation and indistinct nature of the spine near resonance may lead to inaccuracies, as discussed above. The different losses predicted by linear and nonlinear theories in the steady state are readily determined by comparing their respective loop areas in Fig. 19, Row 3. Of particular interest is Fig. 19(c), where the nonlinear model displays a second harmonic (which is of course not apparent in the linear result). In calculating the losses, the area of the clockwise loops must be subtracted from the anticlockwise loops.[49] Clearly, when bubbles undergo nonlinear pulsations, the propagation conditions may be very different from the predictions of linear theory.

Given that bubbles can generate nonlinearities during acoustic propagation of high amplitude fields, one may speculate on how this might offer a solution to the question of whether dolphins could have a way of using sonar effectively in the bubble nets they generate. It is very likely that, if dolphin sonar really does operate effectively in bubbly water, the dolphins must mentally be undertaking signal processing which takes into account the nonlinearities that they are generating. This is because dolphins are able to echolocate in environments (e.g. some sediment suspensions) which confound the best human sonar systems; but their sonar parameters (e.g. beam patterns and source levels) are inferior to those of the best man-made sonar systems.[127] Therefore, it is the processing undertaken by these dolphins which must be making the difference. Given the severe scattering, attenuation and reverberation the dolphin must be counteracting, a nonlinear process would seem to be a strong possibility. Certainly, the high amplitudes and short ranges involved in the use of dolphin sonar in bubble nets would promote the possibility of generating nonlinearities. Note that the high attenuations calculated at the start of this section rely on the assumption of linear steady-state monochromatic insonification, and dolphins can operate outside this regime.

Consider the following thought-experiment, where one wishes to use sonar to detect a linear scatterer, given that there is a bubble cloud in the propagation path. Such a linear scatterer might be a fish, with or without a swim bladder (which at sufficiently high frequencies would behave linearly) within a dolphin bubble net. Alternatively, it might be a solid object, such as a mine, hidden near-shore where its presence presents a hazard to landing craft, such that even without detonating, it can seriously interfere with marine activity. Sonar attempts to detect such a mine fail because the returned sonar signal is dominated by the scatter from the bubble clouds in the vicinity of the mine, generated by breaking waves.

Consider if the scatter from the bubbles were linear. In this case, all that could be done to suppress the overwhelming contribution from the bubbles in the detected signal, would be to try to exploit the time-dependence of the signal. This has proved to have very limited success to date.[1,125,128–130] However, if the amplitude of the insonifying field were to be high enough to generate a nonlinear response, it might be possible to enhance scatter from the mine, whilst simultaneously suppressing it from the bubbles. Consider an insonifying field consisting of two high amplitude pulses, one having reverse polarity with respect to the other (Fig. 20, top line). Linear reflection from the linearly scattering body (which we shall call the "target") is shown in Fig. 20b(i). The bubble generates nonlinear radial excursions (Fig. 20a(i)) and emits a corresponding pressure field (Fig. 20a(ii)) (which for this simple illustration is assumed to be dominated by the even-powered nonlinearities, a point to be investigated further in a later publication[1]). Normal sonar would not be able to detect the signal from the target (Fig. 20b(i)) as it is swamped by that from the bubbles (Fig. 20a(ii)).

If, however, the returned time histories are split in the middle and combined to make a time history half as long, enhancement and suppression occurs. If the two halves of the returned signals are added, the scattering from the bubble is enhanced (Fig. 20a(iii) and Fig. 20a(iv)), whilst the scatter from linear scatterers (such as the target) is suppressed (Fig. 20b(ii)). This can be used to enhance the scatter from biomedical contrast agents. If, however, the two halves of each returned signal are subtracted from one another, the scattering from the bubbles is suppressed (Figs. 20a(v) and Fig. 20a(vi)) whilst the reflections from the target are doubled (Fig. 20b(iii)).

The hypotheses of this section are of course preliminary and speculative, with corollaries in the literature.[1] To test whether dolphins do indeed exploit such methods is not as simple an operation as looking for the idealised pulses of Fig. 20, since there is a clearly an infinite class of high-amplitude pulses which would enhance sonar in this manner. Nevertheless, an investigation to see whether dolphins change their output when placed in bubbly environments, and if they do, what pulses do they use, would be very interesting. What is certain is that for creatures which use echolocation underwater, bubbles will contribute a fascinating and potentially confusing environment in which to operate. This would particularly be the case close to shore, where in addition to the clouds of bubbles generated by breaking beach waves, the sloping seabed could appear to produce a wedge-shaped underwater equivalent

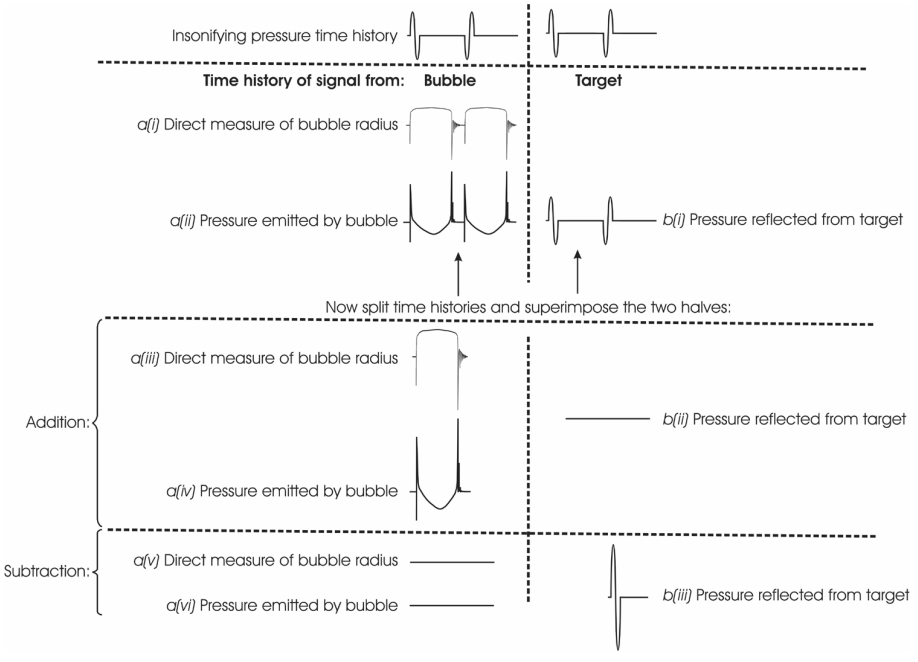

Fig. 20. Schematic of a proposed "Twin Inverted Pulse Sonar", whereby the scattering from a linear scatterer (such as a mine or prey) and scattering from nonlinear scatterers (such as bubbles) can be enhanced and suppressed relative to one another. Consider the following problem scenario: Sonar fails to detect a linearly-scattering body (the "target", e.g. mine or prey), because the returned sonar signal is dominated by the scatter from bubble clouds in the vicinity of the target. If the insonifying field were sufficiently high-amplitude to generate nonlinear response, it might be possible to enhance scatter from the target whilst simultaneously suppressing it from the bubbles. Consider if the insonifying field consisted of two high amplitude pulses, one having reverse polarity with respect to the other (top line). Linear reflection from the target is shown in b(i). The bubble generates nonlinear radial excursions (a(i)) and emits a corresponding pressure field (a(ii)) (which for this simple illustration is assumed to be dominated by the even-powered nonlinearities, a point to be investigated further in a later publication[1]). Normal sonar would not be able to detect the signal from the target (b(i)), as it is swamped by that from the bubbles (a(ii)). If, however, the returned time histories are split in the middle and combined to make a time history half as long, enhancement and suppression occurs. If the two halves of the returned signals are added, the scattering from the bubble is enhanced (a(iii) and a(iv)), whilst the scatter from linear scatterers (such as the target) is suppressed (b(ii)). This can be used to enhance the scatter from contrast agents. If, however, the two halves of each returned signal are subtracted from one another, the scattering from the bubbles is suppressed (a(v) and a(vi)) whilst the reflections from the target are enhanced (with the usual constraints imposed by increased signal-to-noise ratio) (b(iii)).

of a fairground "hall of moving mirrors".[16] It is remarkable that cetaceans can operate in an environment which confounds human sonar.

6. Bubble Acoustics in Processing

As outlined in Sec. 2, by the time of Lord Rayleigh's 1917 publication,[47] a body of interest in bubble collapse had built up. As he wrote:

> When reading O. Reynolds's description of the sounds emitted by water in a kettle as it comes to the boil, and their explanation as due to the partial or complete collapse of bubbles as they rise through cooler water, I proposed to myself a further consideration of the problem thus presented; but I had not gone far when I learned from Sir C. Parsons that he also was interested in the same question in connexion with cavitation behind screw-propellers, and that at his instigation Mr S. Cook, on the basis of an investigation by Besant, had calculated the pressure developed when the collapse is suddenly arrested by impact against a rigid concentric obstacle.

Indeed, the earliest form of this calculation was probably that given by Stokes[131] in an examination question in 1847 (see web page[67] for details).

In these early considerations, the bubble collapse was the result of hydrodynamic forces. If such processing is desirable, it is most conveniently undertaken today through the use of ultrasonics (e.g. in a commercial ultrasonic cleaning

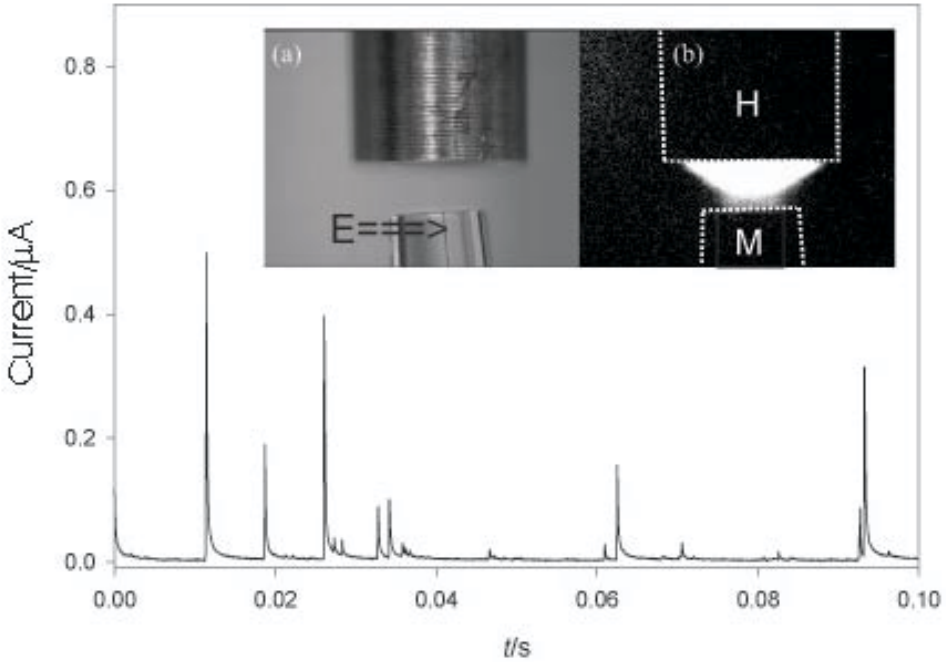

Fig. 21. Plot showing the current recorded as a function of time for a vertical stainless steel microelectrode (25 μm diameter, arrowed as E===> and surrounded by transparent insulation) exposed to inertial cavitation. Individual transients are caused by surface erosion as a result of inertial collapse. The inset images show the ultrasonic horn (H) positioned above a microelectrode (M) taken (a) in external illumination, and (b) with no external illumination. The horn diameter is 3 mm. The light in (b) shows in the image intensifier record of sonoluminescence. The position of the horn (H) and microelectrode (M) are indicated with dotted lines (Figure courtesy of P. R. Birkin, D. Offin and T. G. Leighton). For further details, see the associated web page.[67]

bath[132]). Cavitation erosion can now be monitored on the microsecond timescale (Fig. 21), as opposed to the minute/hour timescales available only a decade ago. One phenomenon which has also opened up monitoring on the sub-second timescale, including the cavitation erosion of blades,[133] is the light emissions associated with energetic bubble collapse (e.g. cavitation luminescence, sonoluminescence or chemiluminescence).[67,134–137] These have proved useful in monitoring the potential for cavitation to generate physical, chemical and biological effects. This is in part because, in addition to providing temporal resolution, luminescence indicates the location of such bubble collapses (Fig. 21). The spatial occurrence of luminescence indicates which regions of a sample are being

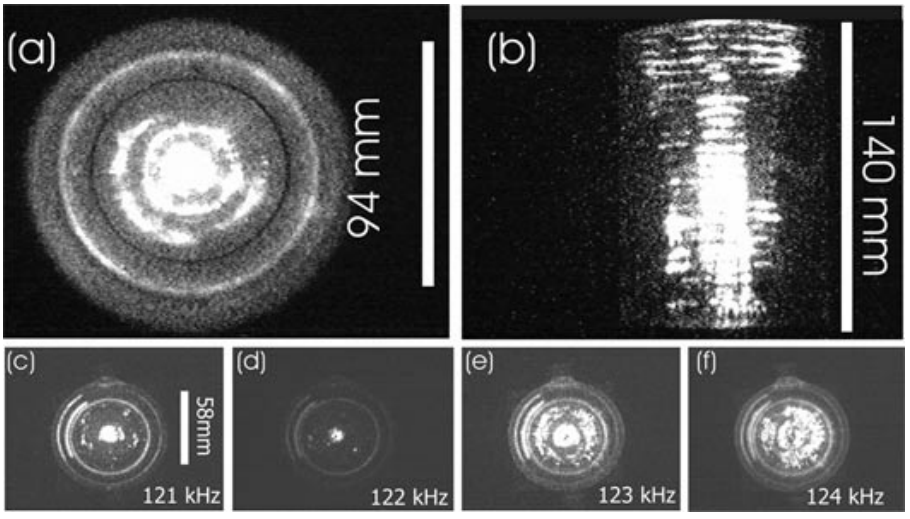

Fig. 22. The acoustic pressure antinodes within reverberant water-filled cylinders (with vertical axis of symmetry, and the sound source at the cylinder base) are made visible through the chemiluminescence which occurs there. (a) Plan and (b) side views of luminescence (which occurs at pressure antinodes) in a water-filled cell which had a polymethylmethacrylate wall (9.4 cm internal diameter, 10 cm external diameter; height of aqueous solution = 14 cm) for insonification at 132.44 kHz where the spatial peak acoustic pressure in the liquid was 75 kPa (all quoted zero-to-peak). Frames (c)–(f) (to which the scale bar of length 5.8 cm in frame (c) refers) were taken in a double-walled, water-jacketed cell (5.8 cm internal diameter, 8.5 cm external diameter, and liquid height 8 cm in a cell which is 12 cm tall) which was maintained at a constant liquid temperature of 25°C. As the insonifying frequency changed, so too did the spatial peak acoustic pressure, providing the following combinations: (c) 121 kHz; 139 kPa; (d) 122 kHz; 150 kPa; (e) 123 kHz; 180 kPa; and (f) 124 kHz; 200 kPa. The effect of tuning into particular acoustic modes is evident: a 1 kHz change in frequency can dramatically alter the amount and distribution of the luminescence. Hence the not uncommon practice of incrementing frequencies by O(100 kHz) when testing for the "optimal processing frequency" in such arrangements is nonsensical. By noting the modal resonance frequencies in these and similar cylinders, the sound speed in this bubbly water was found to be in the range 868–1063 m/s, implying void fractions of $2.9 - 4.2 \times 10^{-3}$ %. Frames selected from several figures in Ref. 138. For further details, see the associated web page.[67] (Figure courtesy of P. R. Birkin, J.F. Power, T. G. Leighton and A. M. L. Vincotte).

processed, and how this changes with frequency[138,139] (Fig. 22). In an example sequence of studies, once sonoluminescence in a given system had been correlated to cell death,[140–142] systems for enhancing and suppressing sonoluminescence have implications for controlling[143–147] biohazard, which may be unwanted (e.g. during foetal scanning[148,149]) or desired (e.g. in dental ultrasonics[150,151]), particularly if the difficult translation to the *in vivo* scenario can be made.[152]

The field of lithotripsy provides another good example of the pattern of investigation described above. That is to say, starting from the correlation of

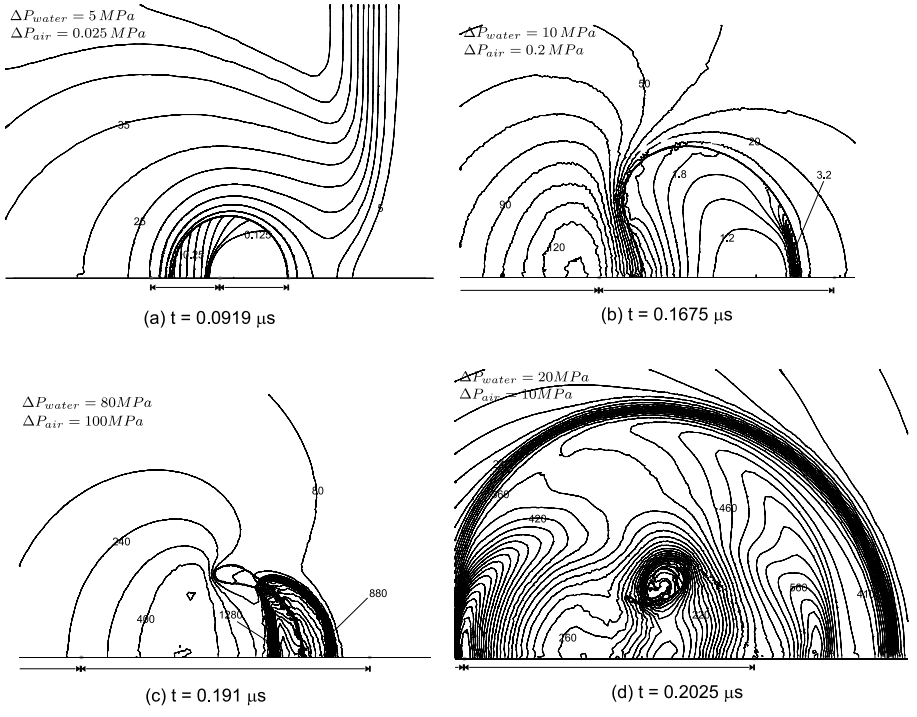

Fig. 23. An air bubble of initial radius 40 microns in water is subjected in the free field to a lithotripter pulse (propagating from left to right). The response is predicted by the Vucalm hydrocode,[159–162] the axis of rotational symmetry being the horizontal line at the base of each plot. Two 20-micron arrows (or parts thereof), parallel to this under each frame, meet at the initial centre of the bubble. The contour increments in pressure for both air and water are indicated on each plot, the value of selected contours being labelled in MPa. All elapsed times "t" are measured after the lithotripter pulse first meets the upstream bubble wall. (a) The lithotripter pulse has passed over the bubble, travelling further than the slower gas shock within the bubble. An expansion wave is reflected back off the bubble, travelling to the left and upwards in the picture. (b) The bubble involutes as it collapses, to form a liquid jet which will pass through the centre of the bubble. (c) The impact of the jet against the downstream bubble wall generates a blast wave which propagates outwards in (d). Such liquid impacts and blast waves can generate erosion and biomechanical effects. The high temperatures and pressures attained within the gas can generate chemical effects and luminescence (Image courtesy of A. R. Jamaluddin, C. K. Turangan, G. J. Ball and T. G. Leighton). For further details and animations, see the associated web page.[67]

cavitation with a biophysical parameter via sonoluminescence, the study has progressed through *in vitro*[153–156] and *in vivo* experimentation to an eventual clinical application.[1] Lithotripsy is a clinical procedure in which thousands of shock waves, generated by a shock wave source at intervals of roughly one per second, are focused onto kidney stones in order to break them up into fragments small enough to be naturally passed from the body or dissolved by drugs. The shock-induced formation and collapse of bubbles in the vicinity of the stone is thought to be an important component in the fracture process. Recently a device for passively monitoring the degree of stone fragmentation *in vivo* has undergone clinical trials. It operates by monitoring the passive acoustic emissions which reverberate in the human body following the passage of each shock wave.

Sonoluminescence played an important part in the early development of the method. In the 1990s, a correlation between the sonoluminescent and the passive acoustic emissions, identified cavitation as the source of that acoustic emission.[157,158] How these passive emissions arise from the interaction between the incident shock, the kidney stone and the bubbles, and what they can tell us about the effectiveness of each lithotripsy procedure, were identified using Computational Fluid Dynamics[1,159–162] (Fig. 23). This enabled the design of prototype monitors[154–156,163,164] and, after *in vitro* and *in vivo* testing, to clinical trials (Fig. 24; for further details see the associated web page[67]). Although lithotripsy is in most cases far preferable to the surgical removal of kidney stones, there is currently no method of monitoring the degree of stone fragmentation. As a result, patients are subjected to a preset number of shocks (several thousand). If too few are given, re-treatment is necessary. If too many shocks are given, unnecessary exposure and collateral tissue damage may occur. In addition, the expensive shock wave sources have a lifetime limited by the number of firings. The ability to limit the number of shocks to the number required for adequate stone fragmentation would conserve hospital resources, both financially and in terms of waiting times. This resulting "smart stethoscope" grew from a study of the fundamental physics, and has produced a device which has tested well in the clinic.[1]

In the above examples, processing took place through jet impact, and blast waves, and chemical effects when compressed gas within the collapsing bubble attains temperatures in excess of about 6000 K (the temperature of the surface of the sun), and generates highly reactive chemical species. These effects are characteristic of inertial (or transient[2,42,134,165–168]) cavitation, and hence require acoustic pressure amplitudes greater than 100 kPa (Earth standard surface conditions). Not all processing requires this. For example, whilst many industries inject gas into liquids to promote mass flux, some are researching the use of >100 kPa acoustic fields to promote mass flux through inertial cavitation. However, initial studies[169] have demonstrated that, by exciting Faraday waves in a bubble wall (see below), one tenth of the mass flux that was generated through inertial cavitation, can be generated with sound fields of only 10–100 Pa acoustic pressure amplitude (a local reduction in acoustic power of $10^6 - 10^8$). Clearly, the prospect of

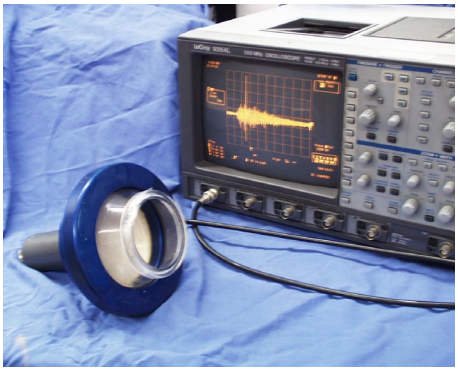

(a)

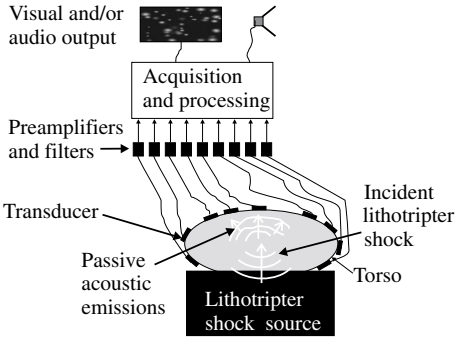

(b)

(c)

Fig. 24. (a) Photograph of an early prototype passive cavitation detector, with typical cavitation emissions displayed. This device consisted of a bowl hydrophone, resonant at 1 MHz, which was placed on the patient and allowed *in vivo* monitoring of acoustic emissions resulting from cavitation during lithotripsy. (b) Schematic for the operation of the broadband clinical prototype[163] passive cavitation detector. The lithotripter focuses a shock wave onto the kidney stone from below. Broadband sensors placed on the torso detect the passive acoustic emissions, and these are processed to give feedback to the clinician (either in audio form, or as a display) on the targeting of the lithotripter, on the cavitation which occurs *in vivo*, and on the degree of stone fragmentation.[164] (c) The finished prototype (Manufactured by Precision Acoustics Ltd., A. Hurrell engineer) being used in the clinic (Guy's and St Thomas' NHS Foundation Trust, London). The figure shows the author (right), his student F. Fedele (middle) and radiographer H. Keerasekera monitoring a patient (blanked out for reasons of confidentiality) during lithotripsy treatment at Guy's Hospital. A single sensor is deployed here, rather than the array shown in part (b), but it gives excellent results. For further details, including recordings of the sounds detected by the device in the clinic, see the associated web page[67] (Images courtesy of T. G. Leighton and A. J. Coleman (co-investigator on the project)).

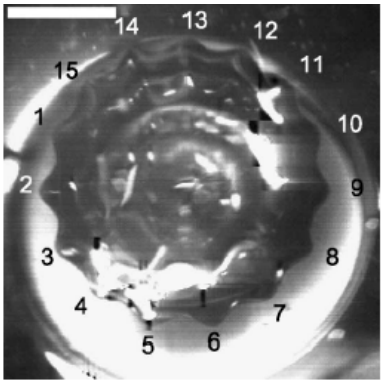

Fig. 25. View from below an air bubble, restrained against buoyant rise by a glass rod, visible as the white circle "behind" the bubble (scale bar: 2 mm). The bubble (of radius ∼2.5 mm) was driven into oscillation by an acoustic driving field. Such fields will always excite the pulsation mode, but if the bubble wall pulsation amplitude is sufficiently great, instabilities on the bubble wall grow rapidly. The mode which requires the lowest amplitude of pulsation to excite corresponds to the Faraday wave. Here, the bubble was driven at 1.297 kHz, with 83.5 Pa zero-to-peak acoustic pressure amplitude. This is enough to stimulate just the Faraday wave (the order 15 spherical harmonic perturbation, annotated), and of course the breathing mode (order zero). The wall displacements associated with the breathing mode are micron-order, much smaller than the Faraday wave, which therefore gives the larger visual signal. However the acoustic emission by the bubble is dominated by the monopole breathing mode, even though the greater wall displacements of the Faraday wave generate fluid currents much larger than those resulting from the breathing mode. This can be seen in Fig. 28 (Image courtesy of P. R. Birkin, Y. E. Watson and T. G. Leighton). For further details, see the associated web page.[67]

translating even a fraction of this efficiency gain to industry is exciting. Moreover, this new field of acoustoelectrochemistry[170–174] offers fundamental research into the formation of surface waves on bubble walls (Fig. 25). These grow parametrically when the acceleration in the plane normal to a liquid/gas interface exceeds a threshold value, as first demonstrated by Faraday himself (Fig. 26(a)). As he writes[175]:

> When the upper surface of a plate vibrating so as to produce sound ... is covered with a layer of water, the water usually presents a beautifully crispated appearance in the neighbourhood of these centres of vibration ... they are seen to be conoidal heaps rounded above, and apparently passing into each other below by a curvature in the opposite direction.

For accelerations just exceeding the threshold, only one mode is excited (Fig. 26(b)), the one having a frequency half that of the driver. It is this wave which is known as the Faraday wave. However, each of the other surface modes has a higher threshold, so that as the acceleration increases further, more modes are excited (Fig. 26(c)), complicating the surface motion. This eventually results in droplet formation in Fig. 26(c), the corresponding phenomenon being bubble fragmentation (Fig. 27).

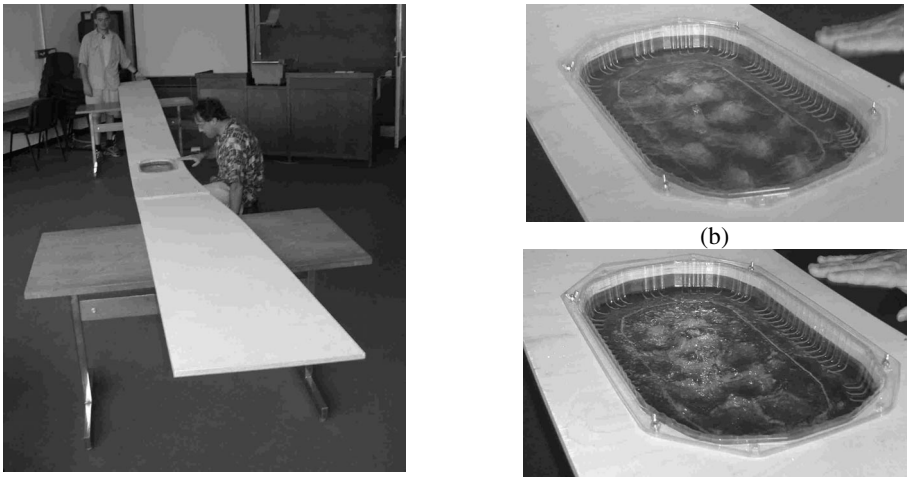

Fig. 26. (a) The author and a technician (D. Theobald) experiment with a replica of the 18 ft plank of wood with which Faraday[175] generated and studied the formation of surface waves on liquids undergoing acceleration normal to the gas/liquid interface (Photo: G. Farrell). (b) Regular "crispations" generated at low driving amplitude. (c) Splashing generated at higher driving amplitudes. Video clips can be accessed via the associated web page.[67]

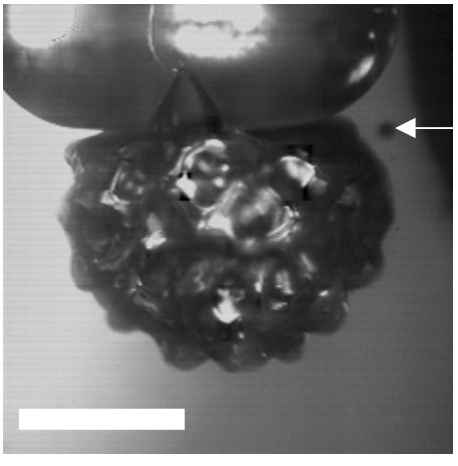

Fig. 27. Picture showing the fragmentation of a gas bubble ($\sim$ radius 2.1 mm) driven at 1.5006 kHz (139 Pa). The arrow shows a small bubble fragmenting off the main bubble. The scale bar represents 2 mm (Courtesy of P. R. Birkin, Y. E. Watson and T. G. Leighton).

Such surface waves may be detected electrochemically (Fig. 28), which has allowed characterisation and measurement of the threshold conditions, and even examination of the chaotic growth[176,177] of the modes (Fig. 29). Faraday describes the process thus[175]:

> As to the origin ... the smallest possible difference in almost any circumstance, at any one part, would, whilst the plate is vibrating, cause an elevation or depression in the fluid there; the smallest atom of dust falling on the surface, or the smallest elevation in the plate, or the smallest particle in the fluid of different specific gravity to the liquid itself, might produce this first effect; this would, by each vibration of the plate, be increased in amount ... so that in less than a second a large surface would be affected.

7. The Future for Bubble Acoustics

There are great opportunities for fundamental and applied research into the physical, chemical and biological implications of bubble acoustics. Phenomena from the range described in this article could be used as the basis of speculative extrapolation towards future directions of research. To give one example, Fig. 3 illustrated the ability of contrast agents to provide localised enhancement in ultrasonic im-

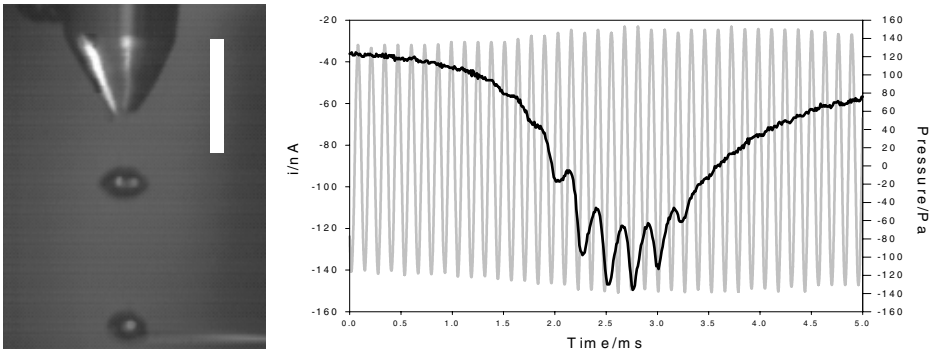

Fig. 28. Bubbles are injected into a sound field, and rise under buoyancy towards an electrochemical microelectrode. In the photograph (scale bar = 2.2 mm), the horizontal injection needle can just be seen at the bottom right corner and the downwards-facing microelectrode can be seen at the top of the picture. The microelectrode produces current as a result of mass transfer related to the presence of 5 mmol dm^{-3} $K_3Fe(CN)_6$ in 0.1 mol dm^{-3} $Sr(NO_3)_2$, the sensing area being 25 μm diameter of Platinum at the electrode tip. Hence, most of the "microelectrode" which is visible on the photograph is the glass insulating surround. Two bubbles can be seen, the twin highlights on the upper one indicating peaks of Faraday waves (as in Fig. 25). The graph shows, against a common time axis, the insonifying sound field (grey line) and the electrochemical current (black line). Flow (caused here by bubble motion, which in this experiment comprises translation, pulsation and Faraday wave) tends to disrupt the depletion layer that forms around the microelectrode tip. Therefore, the current tends to increase in magnitude as the bubble moves close to the microelectrode. Such an increase is seen as the bubble approaches the needle, followed by a decrease as the bubble continues its buoyant rise above the microelectrode. At its closest approach, the current clearly shows an oscillation at the subharmonic of the driving sound field, this subharmonic being the frequency at which the Faraday waves on the bubble wall oscillate. This is of course at half of the 7.678 kHz fundamental of the driving field (grey line) at which the breathing mode oscillates. Hence, the higher order mode generates a much larger electrochemical signal, although the breathing mode dominates the acoustic signal (Photographs and data courtesy of P. R. Birkin, Y. E. Watson, J. Flemming and T. G. Leighton). For further details, see the associated web page.[67]

ages. The bubble walls of contrast agents are already engineered to provide bubble longevity. Further engineering might make the bubbles attach to specific cells, so that contrast agents injected throughout the body might accumulate at specific target sites. This could not only enable identification of the locality of specific types of cells (e.g. tumour cells) in the body, through "hot spots" in ultrasound images. It would also place within the locality of those cells a microbubble which could be excited to process the cell (by, for example, injecting material from within the bubble into the cell at the tip of the liquid jet which forms as the bubble collapses — Figs. 23 and 30).

The ability of bubbles to change their environment chemically would appear to possess great potential for industry. However, the commercial exploitation of these effects is restricted primarily by the limited consideration given to the physics,[138,139,178–180] and particularly the acoustics, by many studies in chemical or material processing by ultrasound (see, for example, the caption to Fig. 22). This has given the field the unwarranted reputation of irreproducibility and the inability to scale-up. Sonochemists are in the habit of referring to their field as a

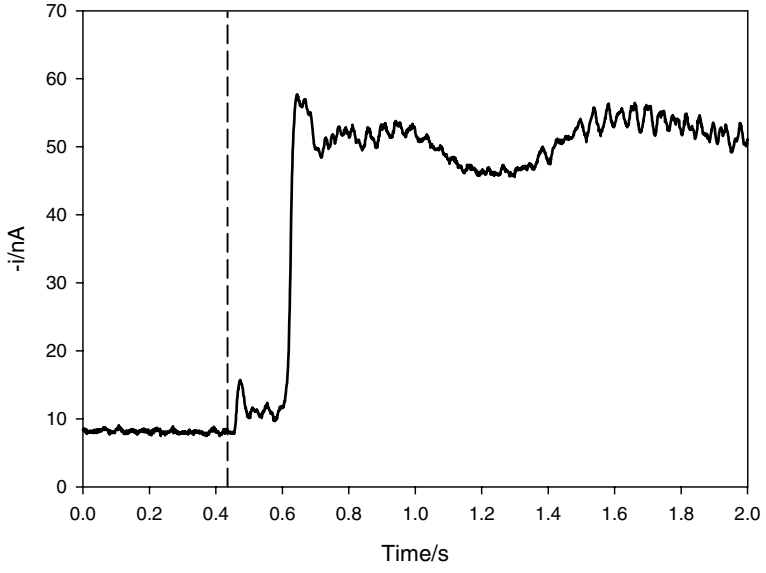

Fig. 29. Plot illustrating the current time history recorded as surface waves grow upon the wall of an insonified bubble. The onset of insonification is indicated by the vertical dashed line. The current time history was recorded by a 25 μm Pt microelectrode in 5 mmol dm^{-3} $Fe(CN)_6^{3-}$/0.2 mol cm^{-3} $Sr(NO_3)_2$ positioned close to an air bubble in the presence of a sound field of 2.048 kHz at 38.45 Pa (measured in the absence of the bubble). To record 2 s of data, the sampling rate was 1 kHz, which is insufficient to resolve the 2.048 kHz fundamental or its subharmonic. However, it captures the ∼40 nA step in current caused by the growth of Faraday waves, and the initial ∼5 nA "spike" in current which is always seen shortly after the onset of insonification. The lower frequency (∼1 Hz) signals after the current step are not uncommon, and related to translational motion of the bubble (Courtesy of P. R. Birkin, Y. E. Watson, T. G. Leighton).

Fig. 30. Jet formation during the collapse of an oscillating gas-vapour bubble at low pressure (4–5 kPa) in a 60 Hz sound field. The bubble size is approximately 0.2 cm (Photograph courtesy of LA Crum). For further details, see the associated web page.[67]

"black art". It is not so, but rather it is multidisciplinary and requires in-depth appreciation of both the chemistry and the physics.

Acknowledgments

The author would like to thank the Royal Society Leverhulme Trust for a Senior Research Fellowship, and the EPSRC for research funding (GR/R12695/01, GR/S78698/01, GR/N19243/01, GR/N30989/01, GR/S01764/01). The author is very grateful to Peter Birkin, Simon Richards, Siân Lloyd Jones, Phil Nelson and Victor Humphrey for test-reading this article.

References

1. T. G. Leighton, *Bubble Acoustics from Seas to Surgeries*, to appear in *Springer Series in The Modern Acoustics and Signal Processing Series* (Springer, USA, 2005).
2. T. G. Leighton, *The Acoustic Bubble* (Academic Press, UK, 1994).
3. R. D. Watkins, L. M. Barrett and J. A. McKnight, *Nucl. Energy* **27**, 85 (1988).
4. N. Lions *et al.*, Special instrumentation for Phenix. Fast reactor power stations (Thomas Telford, London, 1984), pp. 525–535.
5. C. K. Day and R. W. Smith, *IEEE Trans*, SU-21, No. 3 (1974).
6. J. A. McKnight *et al.*, *Ultrasonics International 83* (Butterworth Scientific, UK, 1983), pp. 135–140.
7. J. A. McKnight *et al.*, Recent advances in the technology of under-sodium inspection in LMFBRs. Liquid metal engineering and technology. BNES, London, **1**, 423 (1984).
8. A. Aguilar and G. Por, *Ann. Nucl. Energy* **14**, 521 (1987).
9. T. L. Szabo, *Diagnostic Ultrasound Imaging: Inside Out* (Elsevier Science, Boston, 2004).
10. E. R. Hughes, T. G. Leighton, G. W. Petley and P. R. White, *Ultrasound in Med. and Biol.* **25**(5), 811 (1999).
11. C. F. Njeh, D. Hans, T. Fuerst, C. C. Gluer and H. K. Genant, *Quantitative Ultrasound: Assessment of Osteoporosis and Bone Status* (Martin Dunitz, London, 1999).

12. C. M. Langton, S. B. Palmer and R. W. Porter, *Eng. in Med.* **13**(2), 89 (1984).
13. E. R. Hughes, T. G. Leighton, G. W. Petley, P. R. White and R. C. Chivers, *Ultrasonics* **41**, 365 (2003).
14. A. Hosokawa and T. Otani, *J. Acoust. Soc. Am.* **101**, 558 (1997).
15. E. R. Hughes, T. G. Leighton G. W. Petley and P. R. White, *Acoust. Bulletin* **26**(5), 17 (2001).
16. T. G. Leighton and G. J. Heald, Chapter 21: Very high frequency coastal acoustic, in *Acoustical Oceanography: Sound in the Sea*, ed. H. Medwin (Cambridge University Press, UK, 2005).
17. H. Medwin *et al.*, *Acoustical Oceanography: Sound in the Sea* (Cambridge University Press, UK, 2005).
18. H. Medwin and C. S. Clay, *Fundamentals of Acoustical Oceanography* (Academic Press, USA, 1998).
19. T. G. Leighton (ed.), *Natural Physical Processes Associated With Sea Surface* (University of Southampton, UK, 1997).
20. T. G. Leighton, G. J. Heald, H. Griffiths and G. Griffiths (eds.), *Acoustical Oceanography*, in *Proc. of the Institute of Acoustics* **23** Part 2 (Bath University Press, UK, 2001).
21. D. V. Holliday, Acoustical sensing of biology in the sea, *Acoustical Oceanography*, in *Proc. of the Institute of Acoustics* **23** Part 2, eds. T. G. Leighton, G. J. Heald, H. Griffiths and G. Griffiths (Bath University Press, UK, 2001), pp. 172–180.
22. J. K. Dix, S. Arnott, A. I. Best and D. Gregory, The acoustic characteristics of marine archaeological wood, *Acoustical Oceanography*, in *Proc. of the Institute of Acoustics* **23** Part 2, eds. T. G. Leighton, G. J. Heald, H. Griffiths and G. Griffiths (Bath University Press, UK, 2001), pp. 299–305.
23. J. M. Smith, Coastal Engineering 2002 Solving Coastal Conundrums, (3 Volumes), in *Proc. of the 28th International Conference* (World Scientific, Singapore, 2002).
24. D. H. Peregrine, *Ann. Rev. Fluid Mech.* **15**, 149 (1983).
25. M. S. Longuet-Higgins and J. S. Turner, *J. Fluid Mech.* **63**, 1 (1974).
26. M. S. Longuet-Higgins, *J. Acoust. Soc. Am.* **87**(2), 652 (1990).
27. D. H. Peregrine, *Ann. Rev. of Fluid Mech.* **35**, 23 (2003).
28. G. Rehder, P. W. Brewer, E. T. Peltzer and G. Friedrich, *Geophysical Research Letters* **29**, 21 (2002).
29. I. Leifer and A. G. Judd, *Terra Nova* **14**(6), 417 (2002).
30. J. Greinert, Y. Artemov, L. Naudts and M. De Batist, Methane "bubble" seeps in the Black Sea and approaches for hydroacoustic methane flux determination, in *Proc. of the Seventh European Conference on Underwater Acoustics*, ed. D. G. Simons (Delft University of Technology, The Netherlands, 2004), pp. 863–868.
31. P. S. Liss and R. A. Duce, (eds.) *The Sea Surface and Global Change* (Cambridge University Press, UK, 1997).
32. I. Anderson and S. Bowler, *New Scientist* **125**, 1707 (1990).
33. E. G. Tickner, Precision microbubbles for right side intercardiac pressure and flow measurements, in *Contrast Echocardiography*, eds. R. S. Meltzer and J. Roeland (Nijhoff, London, 1982).
34. M. L. Denbow, A. W. Welsh, J. M. Taylor, M. J. K. Blomley, D. O. Cosgrove and N. M. Fisk, *Radiology* **214**, 724 (2000).
35. G. Ter Haar (personal communication).
36. D. R. Gross, D. L. Miller and A. R. Williams, *Ultrasound Med. Biol.* **11**, 85 (1985).
37. E. O. Belcher, *IEEE Trans. Biomed. Eng.* **27**, 330 (1980).
38. H. Kisman, *Ultrasonics* **15**, 105 (1977).

39. D. Dowson, A. Unsworth and V. Wright, *Proc. Tribology Conv.* (London: Inst. Mech. England, 1971), pp. 120–127.
40. D. Dowson, A. Unsworth and V. Wright, *Ann. Rheumatic Dis.* **30**, 348 (1971).
41. D. Dowson, A. Unsworth and V. Wright, *Ind Lub Tri* **26**, 212 (1971).
42. R. E. Apfel, Methods in Experimental Physics Vol. 19, ed. P. D. Edmonds (Academic Press, New York, 1981), pp. 355–413.
43. P. M. Shankar, J. Y. Chapelon and V. L. Newhouse, *Ultrasonics* **24**, 333 (1986).
44. H. J. M. Hulshof and F. Schurink, *Kema Scientific and Technical Reports* **3**, 61 (1985).
45. R. M. Detsch and R. N. Sharma, *The Chem. Eng. J.* **44**, 157 (1990).
46. T. J. Lin and H. G. Donnelly, *AIChE J.* **12**, 563 (1966).
47. L. Rayleigh, *Phil. Mag.* **34**, 94 (1917).
48. T. G. Leighton, *J. Acoust. Soc. Am.* **110**(5) Part 2, 2694 (2001).
49. T. G. Leighton, S. D. Meers and P. R. White, *Proc. of the Royal Soc.* **A460**(2049), 2521 (2004).
50. M. S. Longuet-Higgins, *J. Fluid Mech.* **201**, 525 (1989).
51. M. S. Longuet-Higgins, *J. Fluid Mech.* **201**, 543 (1989).
52. M. S. Longuet-Higgins, *J. Fluid Mech.* **224**, 531 (1991).
53. M. S. Longuet-Higgins, *J. Acoust. Soc. Am.* **91**, 1414 (1992).
54. T. G. Leighton and A. J. Walton, *Eur. J. of Phys.* **8**, 98 (1987).
55. M. R. Loewen and W. K. Melville, *J. Acoust. Soc. Am.* **90**, 2075 (1991).
56. J. A. Nystuen and M. J. McPhaden, The beginnings of operational marine weather observations using underwater ambient sound, *Acoustical Oceanography*, in *Proc. of the Institute of Acoustics*, **23** Part 2, eds. T. G. Leighton, G. J. Heald, H. Griffiths and G. Griffiths, (Bath University Press, UK, 2001), pp. 135–141.
57. T. G. Leighton, M. F. Schneider and P. R. White, Study of bubble fragmentation using optical and acoustic techniques, *Sea Surface Sound 94*, in *Proc. of the 3rd Meeting on Natural Physical Processes related to Sea Surface Sound*, eds. M. J. Buckingham and J. R. Potter (World Scientific, Singapore, 1995), pp. 414–428.
58. R. His, M. Tay, D. Bukur and G. Tatterson, *The Chem. Eng.* **31**, 153 (1985).
59. L. S. De More, W. F. Pafford and G. B. Tatterson, *AIChE J.* **34**, 1922 (1988).
60. J. W. R. Boyd and J. Varley, *AIChE J.* **44**, 1731 (1998).
61. A. B. Pandit, J. Varley, R. B. Thorpe and J. F. Davidson, *Chem. Eng. Sci.* **47**, 1079 (1992).
62. R. Manasseh, R. F. LaFontaine, J. Davy, I. Shepherd and Y. G. Zhu, *Experiments in Fluids* **30**(6), 672 (2001).
63. T. A. Sutter, G. L. Morrison and G. B. Tatterson, *AIChE J.* **33**, 668 (1987).
64. W. R. Usry, G. L. Morrison and G. B. Tatterson, *Chem. Eng. Sci.* **42**, 1856 (1987).
65. T. G. Leighton, K. J. Fagan and J. E. Field, *Eur. J. of Phys.* **12**, 77 (1991).
66. T. G. Leighton, P. R. White and M. F. Schneider, *J. Acoust. Soc. Am.* **103**, 1825 (1998).
67. http://www.isvr.soton.ac.uk/fdag/ijmpb.htm
68. T. G. Leighton and P. R. White, *Acoust. Bulletin* **29**, 16 (2004).
69. L. L. Foldy, *Phys. Rev.* **67**, 107 (1945).
70. S. G. Kargl, *J. Acoust. Soc. Am.* **111**, 168 (2002).
71. A. Prosperetti, *J Acoust. Soc. Am.* **78**, S2 (1985).
72. W. M. Carey, *J. Acoust. Soc. Am.* **78**, S1 (1985).
73. T. G. Leighton, P. R. White, C. L. Morfey, J. W. L. Clarke, G. J. Heald, H. A. Dumbrell and K. R. Holland, *J. Acoust. Soc. Am.* **112**(4), 1366 (2002).
74. D. L. Miller, *J. Acoust. Soc. Am.* **77**, 946 (1985).

75. R. M. Quain, R. C. Waag and M. W. Miller, *Ultrasound Med. Biol.* **17**, 71 (1991).
76. H. N. Oguz and A. Prosperetti, *J. Acoust. Soc. Am.* **103**, 3301 (1998).
77. X. Geng, H. Yuan and A. Prosperetti, *J. Acoust. Soc. Am.* **106**, 674 (1999).
78. T. G. Leighton, P. R. White and M. A. Marsden, *Eur. J. of Phys.* **16**, 275 (1995).
79. T. G. Leighton, P. R. White and M. A. Marsden, *Acta Acustica* **3**, 517 (1995).
80. T. G. Leighton, D. G. Ramble, A. D. Phelps, C. L. Morfey and P. P. Harris, *Acta Acustica* **84**, 801 (1998).
81. T. G. Leighton, W. L. Ho and R. Flaxman, *Ultrasonics* **35**, 399 (1997).
82. T. G. Leighton, A. D. Phelps, B. T. Cox and W. L. Ho, *Acta Acustica* **84**, 1014 (1998).
83. T. G. Leighton, B. T. Cox and A. D. Phelps, *J. Acoust. Soc. Am.* **107**, 130 (2000).
84. T. G. Leighton, B. T. Cox, P. R. Birkin and T. Bayliss, The Rayleigh-like collapse of a conical bubble: Measurements of meniscus, liquid pressure, and electrochemistry, in *Proc. of the 137th Regular Meeting of the Acoustical Society of America and the 2nd Convention of the European Acoustics Association (Forum Acusticum 99, integrating the 25th German Acoustics DAGA Conference)*, Paper 3APAB_1 (March 1999).
85. D. D. Symons, *Proc. Inst. Mech. Engrs.* **218**, 233 (2004).
86. M. Minnaert, *Phil. Mag.* **16**, 235 (1933).
87. T. G. Leighton, *Environmental Eng.* **7**, 9 (1994).
88. W. Lauterborn and A. Koch, *Phys. Rev.* **A35**, 1974 (1987).
89. T. G. Leighton, A. D. Phelps and D. G. Ramble, *Acous. Bulletin* **21**, 5 (1996).
90. T. G. Leighton, M. D. Simpson, S. D. Meers, P. R. White, G. J. Heald, H. A. Dumbrell, J. W. Clarke, P. R. Birkin and Y. Watson, *J. Acoust. Soc. Am.* **108**(5), Part 2, 2493 (2000).
91. V. G. Welsby and M. H. Safar, *Acustica* **22**, 177 (1968/70).
92. E. A. Zablotskaya and S. I. Soluyan, *Phys. Acoust.* **18**, 396 (1973).
93. D. L. Miller, *Ultrasonics* **19**, 217 (1981).
94. Z. Kluzek, I. A. Soustova and A. M. Sutin, *Acoust. Phys.* **42**, 568 (1996).
95. A. D. Phelps, D. G. Ramble and T. G. Leighton, *J. Acoust. Soc. Am.* **101**(4), 1981 (1997).
96. A. M. Sutin, S. W. Yoon, E. J. Kim and I. N. Didenkulov, *J. Acoust. Soc. Am.* **103**, 2377 (1998).
97. T. G. Leighton, A. D. Phelps, D. G. Ramble and D. A. Sharpe, *Ultrasonics* **34**, 661 (1996).
98. T. G. Leighton, D. G. Ramble and A. D. Phelps, *J. Acoust. Soc. Am.* **101**(5), 2626 (1997).
99. T. G. Leighton, R. J. Lingard, A. J. Walton and J. E. Field, *Ultrasonics* **29**, 319 (1991).
100. A. D. Phelps and T. G. Leighton, *J. Acoust. Soc. Am.* **99**, 1985 (1996).
101. A. D. Phelps and T. G. Leighton, *Acta Acustica* **83**, 59 (1997).
102. P. R. Birkin, Y. E. Watson, K. L. Smith, T. G. Leighton and M. D. Simpson, Measurement of species flux from a bubble using an acousto-electrochemical technique, *Acoustical Oceanography*, in *Proc. of the Institute of Acoustics* **23** Part 2, eds. T. G. Leighton, G. J. Heald, H. Griffiths and G. Griffiths (Bath University Press, UK, 2001), pp. 242–249.
103. P. R. White, W. B. Collis, T. G. Leighton and J. K. Hammond, Detection of bubbles via Higher Order Statistics, *Natural Physical Processes Associated With Surface Sound*, ed. T. G. Leighton (University of Southampton, UK, 1997), pp. 179–185.
104. P. R. White, W. B. Collis and T. G. Leighton, Analysis of bubble scattering data using higher order statistics, in *Proc. of the 3rd European Conference on Underwater Acoustics, Heraklion*, ed. J. Papadakis (1996), pp. 1155–1160.

105. B. Boashash, E. J. Powers and A. M. Zoubir eds., Higher-Order Statistical Signal Processing (Longman, Wiley Halstead Press, Australia, 1995).
106. P. R. White and T. G. Leighton, Exploitation of Higher Order Statistics to compute bubble cloud densities: Evading Olbers paradox, in *Proc. of the Seventh European Conference on Underwater Acoustics* (2004), pp. 223–228.
107. T. G. Leighton, S. D. Meers, M. D. Simpson, J. W. L. Clarke, G. T. Yim, P. R. Birkin, Y. Watson, P. R. White, G. J. Heald, H. A. Dumbrell, R. L. Culver and S. D. Richards, The Hurst Spit experiment: The characterization of bubbles in the surf zone using multiple acoustic techniques, *Acoustical Oceanography*, in *Proc. of the Institute of Acoustics* **23** Part 2, eds. T. G. Leighton, G. J. Heald, H. Griffiths and G. Griffiths (Bath University Press, UK, 2001), pp. 227–234.
108. T. G. Leighton, A. D. Phelps and D. G. Ramble, Bubble detection using low amplitude multiple acoustic techniques, in *Proc. of the 3rd European Conference on Underwater Acoustics, Heraklion*, ed. J. Papadakis (1996), pp. 1143–1147.
109. N. D. Breitz and H. Medwin, *J. Acoust. Soc. Am.* **86**, 739 (1989).
110. D. M. Farmer and S. Vagle, Bubble measurements using a resonator system, in *Natural Physical Processes Associated with Sea Surface Sound*, ed. T. G. Leighton (University of Southampton, UK, 1997), pp. 155–162.
111. D. M. Farmer, S. Vagle and A. D. Booth, *J. Atmos. Ocean Technol.* **15**, 1132 (1998).
112. K. W. Commander and R. J. McDonald, *J. Acoust. Soc. Am.* **89**(2), 592 (1991).
113. T. G. Leighton, Fundamentals of Underwater Acoustics and Ultrasound, Chapter 7 in Volume 1, in *Noise and Vibration*, eds. F. J. Fahy and J. G. Walker (E & FN Spon an imprint of Routledge, London, 1998), pp. 373–444.
114. T. G. Leighton, S. D. Richards and P. R. White, *Acoust. Bulletin* **29**, 24 (2004).
115. F. A. Sharpe and L. M. Dill, *Canadian J. of Zoology-Revue Canadienne de Zoologie* **75**, 725 (1997).
116. Examples available at http://www.groovedwhale.com; http://www.sfu.ca/biology/berg/whale/abcwhale.html; http://students.ceid.upatras.gr/~pirli/whales/whales.html.
117. W. Au, D. James and K. Andrews, *J. Acoust. Soc. Am.* **110**, 2770 (2001).
118. W. W. L. Au, Harbor porpoise (Phocoena Phocoena) acoustics: In memory of Anthony David Goodson, in *Proc. of the Institute of Acoustics Symposium on Bio-sonar and Bioacoustics Systems, Proc. of the Institute of Acoustics* **26**(6), Paper 01 (2004).
119. A. Byatt, A. Fothergill, M. Holmes and S. D. Attenborough, *The Blue Planet* (BBC Consumer Publishing, 2001).
120. T. M. Keevin, G. L. Hempen and D. J. Schaeffer, Use of a bubble curtain to reduce fish mortality during explosive demolition of Locks and Dam 26, Mississippi River, in *Proc. of the Twenty-third Annual Conference on Explosives and Blasting Technique, Las Vegas, Nevada. International Society of Explosive Engineers, Cleveland, OH* (1997) pp. 197–206.
121. B. Würsig, C. R. Greene, Jr. and T. A. Jefferson, *Marine Environmental Res.* **49**, 79 (2000).
122. K. W. Commander and A. Prosperetti, *J. Acoust. Soc. Am.* **85**, 732 (1989).
123. S. D. Meers, T. G. Leighton, J. W. L. Clarke, G. J. Heald, H. A. Dumbrell and P. R. White, The importance of bubble ring-up and pulse length in estimating the bubble distribution from propagation measurements, *Acoustical Oceanography*, in *Proc. of the Institute of Acoustics*, **23** Part 2, eds. T. G. Leighton, G. J. Heald, H. Griffiths and G. Griffiths (Bath University Press, UK, 2001), pp. 235–241.
124. T. G. Leighton, Nonlinear Bubble Dynamics And The Effects On Propagation Through Near-Surface Bubble Layers, High-Frequency Ocean Acoustics, eds.

M. B. Porter, M. Siderius and W. Kuperman (American Institute of Physics, Melville, New York, 2005).
125. J. W. L. Clarke and T. G. Leighton, *J. Acoust. Soc. Am.* **107**(4), 1922 (2000).
126. P. M. Morse and K. U. Ingard, *Theoretical Acoustics* (Princeton University Press, USA, 1986), pp. 874–882.
127. W. W. L. Au, to appear in The Dolphin Sonar: Excellent capabilities in spite of some mediocre properties, in *High-Frequency Ocean Acoustics*, eds. M. B. Porter, M. Siderius and W. Kuperman (American Institute of Physics, Melville, New York, 2005).
128. V. A. Akulichev, V. A. Bulanov and S. A. Klenin, *Sov. Phys. Acoust.* **32**(3), 177 (1986).
129. H. R. Suiter, *J. Acoust. Soc. Am.* **91**, 1383 (1992).
130. N. G. Pace, A. Cowley and A. M. Campbell, *J. Acoust. Soc. Am.* **102**, 1474 (1997).
131. I am grateful to my colleagues at Cambridge University (A. Chakravarty, A. J. Walton and J. E. Field) for bringing this to my attention. Stoke's notebook containing his solution can be found in Cambridge University Library, UK (Add. MS. 7656.NB23).
132. B. Zeqiri, M. Hodnett and T. G. Leighton, A strategy for the development and standardisation of measurement methods for high power/cavitating ultrasonic fields, — Final project report. *NPL Report CIRA(EXT)016 for National Measurement System Policy Unit* (*Department of Trade and Industry*) (January 1997).
133. T. G. Leighton, M. Farhat, J. E. Field and F. Avellan, *J. Fluid Mech.* **480**, 43 (2003).
134. A. J. Walton and G. T. Reynolds, *Advances in Phys.* **33**, 595 (1984).
135. S. Putterman, *Phys. World* **11**, 38 (1998).
136. M. P. Brenner, S. Hilgenfeldt and D. Lohse, *Rev. Mod. Phys.* **74**, 425 (2002).
137. M. Versluis, B. Schmitz, A. von der Heydt and D. Lohse, *Science* **289**, 2114 (2000).
138. P. R. Birkin, T. G. Leighton, J. F. Power, M. D. Simpson, A. M. L. Vincotte and P. F. Joseph, *J. Phys. Chem.* **A107**, 306 (2003).
139. P. R. Birkin, J. F. Power, A. M. L. Vincotte and T. G. Leighton, *Physical Chemistry Chem. Phys.* **5**, 4170 (2003).
140. T. G. Leighton, A. J. Walton and M. J. W. Pickworth, *Eur. J. of Phys.* **11**, 47 (1990).
141. T. G. Leighton, M. J. W. Pickworth, A. J. Walton and P. P. Dendy, *Phys. in Med. and Biol.* **33**(11), 1239 (1988).
142. M. J. W. Pickworth, P. P. Dendy, P. R. Twentyman and T. G. Leighton, *Phys. in Med. and Biol.* **34**(11), 1553 (1989).
143. M. J. W. Pickworth, P. P. Dendy, T. G. Leighton and A. J. Walton, *Phys. in Med. and Biol.* **33**(11), 1249 (1988).
144. M. J. W. Pickworth, P. P. Dendy, T. G. Leighton and E. Worpe, *Phys. in Med. and Biol.* **34**(1), 135 (1989).
145. M. J. W. Pickworth, P. P. Dendy, T. G. Leighton, E. Worpe and R. C. Chivers, *Phys. in Med. and Biol.* **34**(9), 1139 (1989).
146. T. G. Leighton, *Ultrasonics* **27**(1), 50 (1989).
147. T. G. Leighton, A. J. Walton and J. E. Field, *Ultrasonics* **27**, 370 (1989).
148. S. B. Barnett, G. R. ter Haar, M. C. Ziskin, H. D. Rott, F. A. Duck and K. Maeda, *Ultrasound in Med. and Biol.* **26**, 355 (2000).
149. S. Barnett *et al.*, *Ultrasound in Med. and Biol.* **24**, S11 (1998).
150. R. O'Leary, A. M. Sved, E. H. Davies, T. G. Leighton, M. Wilson and J. B. Kieser, *J. of Clin. Periodonol.* **24**, 432 (1997).
151. R. O'Leary, A. M. Sved, E. H. Davies, T. G. Leighton, M. Wilson and J. B. Kieser, *J. of Dental Res.* **74**, 88 (1995).

152. T. G. Leighton, M. J. W. Pickworth, J. Tudor and P.P. Dendy, *Ultrasonics* **28**, 181 (1990).
153. K. B. Cunningham, A. J. Coleman, T. G. Leighton and P. R. White, *Acoust. Bulletin* **26**(5), 10 (2001).
154. F. Fedele, A. J. Coleman, T. G. Leighton, P. R. White and A. M. Hurrell, *Acoust. Bulletin* **29**, 34 (2004).
155. F. Fedele, A. J. Coleman and T. G. Leighton, Use of a cylindrical PVdF hydrophone in a study of cavitation adjacent to stone phantoms during extracorporeal shockwave lithotripsy, in *Proc. of the 9th Annual National Conference of the Institute of Physics and Engineering in Medicine* (Institute of Physics and Engineering in Medicine, UK, 2003), p. 66.
156. F. Fedele, A. J. Coleman, T. G. Leighton, P. R. White and A. M. Hurrell, Development of a new diagnostic sensor for Extra-corporeal Shock-Wave Lithotripsy, in *Proc. of the First Conference in Advanced Metrology for Ultrasound in Medicine, Journal of Physics: Conference Series* **1**, 134 (2004).
157. A. J. Coleman, M. J. Choi, J. E. Saunders and T. G. Leighton, *Ultrasound in Med. and Biol.* **18**, 267 (1992).
158. A. J. Coleman, M. Whitlock, T. G. Leighton and J. E. Saunders, *Phys. in Med. and Biol.* **38**, 1545 (1993).
159. A. R. Jamaluddin, G. J. Ball and T. G. Leighton, Free-Lagrange simulations of shock/bubble interaction in shock wave lithotripsy, in *Proc. of the Second International Conference on Computational Fluid Dynamics, ICCFD, Sydney, Australia* (15–19 July 2002), pp. 541–546.
160. G. J. Ball, B. P. Howell, T. G. Leighton and M. J. Schofield, Shock-induced collapse of a cylindrical air cavity in water: A Free-Lagrange simulation, in *The 22nd International Symposium on Shock Waves, London, Paper 0060*, published April 2000 (July 1999) pp. 1363–1368.
161. G. J. Ball, B. Howell, T. G. Leighton and M. Schofield, Shock-induced collapse of a cylindrical air cavity in water: A Free-Lagrange simulation, *Shock Waves* **10**, 265 (2000).
162. A. R. Jamaluddin, G. J. Ball and T. G. Leighton, Free-Lagrange simulations of shock/bubble interaction in shock wave lithotripsy, in *The 24th International Symposium on Shock Waves, Beijing, China* (in press) (July 20–25, 2003).
163. T. G. Leighton, A. J. Coleman, F. Fedele and P. R. White, A passive acoustic system for evaluating the *in vivo* performance of extracorporeal shock wave lithotripsy, *UK Patent Application No. 0319863.7*.
164. F. Fedele, A. J. Coleman, T. G. Leighton, P. R. White and A. M. Hurrell, A new sensor for detecting and characterising acoustic cavitation *in vivo* during ESWL, in *Proc. of the Institute of Acoustics* **26**, Part 1, p. 422 (2004).
165. H. G. Flynn, Physics of acoustic cavitation in liquids, in *Physical Acoustics*, ed. W. P. Mason (Academic Press, New York, 1964), Vol. 1 Part B, pp. 57–172.
166. H. G. Flynn, *J. Acoust. Soc. Am.* **57**, 1379 (1975).
167. E. A. Neppiras, *Phys. Rep.* **61**, 159 (1980).
168. T. G. Leighton, *Environmental Engineering* **8**, 16 (1995).
169. Y. E. Watson, P. R. Birkin and T. G. Leighton, *Ultrasonics, Sonochemistry* **10**, 65 (2003).
170. P. R. Birkin, T. G. Leighton and Y. E. Watson, The use of Acoustoelectrochemistry to investigate bubble phenomena — Rectified diffusion, in *Proc. of the Fourth International Conference on Applications of Power Ultrasound in Physical and Chemical Processing* (Beasancon, France, 2003), pp. 101–106.

171. P. R. Birkin, Y. E. Watson, T. G. Leighton and K. L. Smith, *Langmuir Surfaces and Colloids* **18**, 2135 (2002).
172. P. R. Birkin, Y. E. Watson and T. G. Leighton, *J. Chem. Soc. Chem. Communications* **24**, 2650 (2001).
173. P. R. Birkin, T. G. Leighton and Y. E. Watson, *Ultrasonics Sonochemistry* **11**(3–4), 217 (2004).
174. P. R. Birkin, T. G. Leighton, Y. E. Watson and J. F. Power, *Acoust. Bulletin* **26**(5), 24 (2001).
175. M. Faraday, *Phil. Trans. Roy. Soc. London* **121**, 319 (1831).
176. A. Maksimov, T. G. Leighton and E. V. Sosedko, Nonlinear Transient Bubble Oscillations, in *Nonlinear Acoustics at the Beginning of the 21st Century* (*Proceedings of the 16th International Symposium on Nonlinear Acoustics*), eds. O. V. Rudenko and O. A. Sapozhnikov (Faculty of Physics, MSU, Moscow, 2002), Vol. 2, pp. 987–990.
177. A. O. Maksimov and T. G. Leighton, *Acta Acustica* **87**(3), 322 (2001).
178. P. R. Birkin, J. F. Power and T. G. Leighton, *J. Chem. Soc. Chemical Communications* **21**, 2230 (2001).
179. P. R. Birkin, J. F. Power, M. E. Abdelsalam and T. G. Leighton, *Ultrasonics Sonochemistry* **10**, 203 (2003).
180. P. R. Birkin, J. F. Power, T. G. Leighton and A. M. L. Vincotte, *Analytical Chemistry* **74**, 2584 (2002).
181. S. D. Richards and T. G. Leighton, Acoustic sensor performance in coastal waters: Solid suspensions and bubbles, *Acoustical Oceanography*, in *Proc. of the Institute of Acoustics* **23** Part 2, eds. T. G. Leighton, G. J. Heald, H. Griffiths and G. Griffiths (Bath University Press, UK, 2001), pp. 399–406.
182. S. D. Richards, T. G. Leighton and N. R. Brown, *Proc. of the Royal Soc.* **A459**, 2153 (2003).
183. N. R. Brown, T. G. Leighton, S. D. Richards and A. D. Heathershaw, Boundary and volume losses in a diffuse acoustic field near the atmosphere/ocean boundary, in *Natural Physical Processes Associated With Surface Sound*, ed. T. G. Leighton (University of Southampton, UK, 1997), pp. 123–132.
184. N. R. Brown, T. G. Leighton, S. D. Richards and A. D. Heathershaw, *J. Acoust. Soc. Am.* **104**(4), 2114 (1998).
185. S. D. Richards and T. G. Leighton, *J. of Defence Sci.* **8**(1), 1 (2003).
186. S. D. Richards, T. G. Leighton and N. R. Brown, *J. Acoust. Soc. Am.* **114**(4), Pt. 1, 1841 (2003).
187. S. D. Richards and T. G. Leighton, *Acoust. Bulletin* **26**(1), 10 (2001).
188. S. D. Richards, Underwater acoustics and sonar performance in turbid environments, in *Proc. of the Institute of Acoustics* **26**, Part 1, pp. 382–393 (2004).
189. S. Thorpe, *Philos. Trans. R. Soc. London* **A304**, 155 (1982).
190. M. S. Longuet-Higgins, *Proc. R. Soc. London* **439**, 611 (1992).
191. H. Williams, Whale Nation, Jonathan Cape, London (1988).
192. T. G. Leighton, M. Wilkinson, A. J. Walton and J. E. Field, *Eur. J. of Phys.* **11**, 352 (1990).